Master Thesis

A survey on descent trajectories from Gateway orbit to the Moon

Jan Wenderoth

Author:	Jan Wenderoth
Matriculation number:	1196421
Course of study:	Aerospace Engineering
Supervisor:	Univ.-Prof. Dr.-Ing. Felix Huber
	Dr. rer. nat. Thomas Andert
	Dr. Dieter Sabath (DLR - Columbus MOS Manager)
	Sofya Spiridonova (DLR - Flight Dynamics Engineer)
	Maximilian Keller (DLR - Flight Dynamics Engineer)
	Carsten Hartmann (DLR - Columbus Operations)
Datum:	August 10, 2023

Affidavit

I hereby declare that I have independently composed this thesis, have not submitted it elsewhere for examination purposes, and have used no sources or aids other than those specified, and that all direct or indirect citations have been duly marked as such.

....

Place, Date

....

Name and Signature

This work was conducted at the Institute of Space Operations and Astronaut Training of the German Aerospace Center (DLR) and supervised by the Chair of Space Operations of the Institute of Spaceflight Engineering and Space Utilization at the Faculty of Aerospace Engineering at the University of the German Federal Armed Forces in Munich.

The translation from German to English was carried out with the help of the Artificial Intelligence Chat GPT developed by OpenAI.

Abstract

Since the end of the Apollo program in 1972, no human has set foot on the Lunar surface. Now, with the start of the Artemis program by National Aeronautics and Space Administration (NASA), a permanent human presence on the Moon is planned. This presence is intended to serve as an outpost for human research and as a launch point for missions deeper into our solar system and to Mars.

To achieve this goal, a station called Gateway is planned to be built, which will orbit around the Moon. The orbit in which it will move has also been specified by NASA. It is a Near Rectilinear Halo Orbit (NRHO) of the L2-Southern-Family with an average radius at pericenter of 3366 km. The orbit has a 9:2 Lunar Synodic Resonance, resulting in an orbital period of approximately 6.5 days. One important reason for choosing this orbit is the absence of eclipses by Earth until at least 2030.

The aim of this thesis is to analyze descent trajectories from the Gateway's orbit to the Lunar surface. For this purpose, both orbital mechanics and operational aspects have been considered. The descent itself has been divided into two parts. The first part consists of the descent from the Gateway's NRHO to three circular parking orbits at an altitude of 100 km. The three orbital planes of the chosen Low Lunar Orbits (LLOs) are orthogonal to each other. Descent trajectories have been calculated using the Python library SEMpy. In the second part of the descent, a landing from the corresponding parking orbits on the Lunar surface has been considered based on theoretical principles.

In the course of the analyses, two case studies, the Orion capsule (NASA) and the Starship (SpaceX), have been examined. The results of the analyses showed that a polar parking orbit is best suited for performing a landing. It was also found that the descent should start as close as possible to the apocenter of the Gateway orbit due to the required change in orbital plane. It was shown that the Orion capsule, with respect to its fuel capacity (full tanks), is only capable of performing the transfer to the parking orbit. The fuel capacity of the Starship (full tanks) is sufficient for a descent to the Lunar surface and an ascent back to a parking orbit.

From an operational point of view, there are hardly any restrictions. However, it should be noted that direct communication with Earth is not possible when the transfer passes behind the Moon from Earth's perspective. Additionally, there may be eclipses of up to half an orbit period on the respective parking orbit.

Contents

Acronyms

CCSDS	Consultative Committee for Space Data Systems
CR3BP	Circular Restricted 3-Body Problem
DLR	Deutsches Zentrum für Luft- und Raumfahrt
ER3BP	Elliptical Restricted 3-Body Problem
ESA	European Space Agency
ESM	European Service Module
LLO	Low Lunar Orbit
NASA	National Aeronautics and Space Administration
NRHO	Near Rectilinear Halo Orbit
TBOBVP	Two-Body Orbital Boundary-Value Problem
USA	United States of America
UTC	Universal Time Coordinated

List of Figures

List of Tables

Chapter 1

Introduction

About 4.5 billion years ago, the Earth collided with the protoplanet Theia. The result of this collision was the celestial body that has fascinated humanity for millennia - the Moon [18]. There is hardly any ancient culture in which the Moon is not part of countless myths and legends. To this day, people look up at the sky at night and are fascinated by the sight that greets them - a brightly shining white sphere.

„And if you are to love, love as the Moon loves; it does not steal the night - it only unveils the beauty of the dark.“ - Isra Al-Thibeh

But the Moon is more than just a shining sphere. Because the knowledge generated through samples of the Lunar surface and the Moon itself using various analysis methods helps researchers around the world to better understand the solar system and even the universe. In addition, the Moon can also serve as a stepping stone for missions deeper into our solar system or even beyond. This is mainly due to the fact that the Moon's gravity is much weaker than that of Earth. Furthermore, there is water on the Moon, which can serve as a basis for life, but can also be used to produce fuel. Another important point that speaks in favor of the Moon as an outpost for humanity is that telescopes of all kinds on the Moon are not disturbed by an atmosphere. However, this is the case on Earth. Because of that, promising research results can also be expected on the Moon concerning this case.

Therefore, it is not surprising that space travel, and specifically programs that have flown to the Moon, enjoy great public and specialized interest. The most famous example of this is probably the Apollo 11 mission by NASA, as on July 20, 1969, the spacecraft Eagle landed on the Lunar surface. This event, as well as Neil Armstrong's radio transmission when he stepped onto the Moon's surface at 21:56 (Houston time), remain world-famous to this day [19].

„That's one small step for a man, one giant leap for mankind.“ - Neil Armstrong

Besides the United States of America (USA), several other nations have also conducted missions to the Earth's natural satellite. Among them is China with its five Chang'E missions to date. India has also advanced research on the Moon with its two Chandrayaan missions, which included orbiters and a rover. Japan has also been involved in Lunar exploration, having sent a technology demonstrator to the Moon in 1990 and successfully conducted the extensive SELENE mission. In addition to these national space agencies, the European Space Agency (ESA) also conducted its first lunar mission in 2003 with the Smart-1 mission. This mission tested, among other things, a solar-electric propulsion system and deep space technology.
Therefore, it is only logical that these and many other space missions have eventually led to the vision of enabling humans to live and work permanently on the surface of the Earth's natural satellite.

To achieve this goal, NASA launched the Artemis program. In addition to establishing a permanent human presence on the Moon, the Artemis program also names the expansion of commercial and international partnerships as an important goal. As a practical consequence of this objective, an unmanned flight around the Moon has already been carried out as part of the Artemis program. The program's planning envisions further manned test flights around the Moon, followed by the first components of a space station to be placed in a Moon-Earth orbit. This station will be called Gateway. From there, astronauts will finally descend to the Lunar surface. After initial test and exploration flights, regular crew and cargo transfers from Earth via Gateway to the Lunar surface are planned to take place [20][21].

1.1 Objectives

The aim of this work is to analyze various descent trajectories from the orbit of the Gateway to the surface of the Moon. These analyses will be conducted from both orbital mechanics and operational perspectives.

For this purpose, trajectories will be initially considered that do not directly represent descent paths to the Lunar surface, but enable a transfer from the orbit of the Gateway to a low circular orbit around the Moon.
In the analysis of these descent paths, fuel consumption or the need for velocity changes will serve as the determining factor. Furthermore, flight time will be taken into account in the considerations.

Following the analysis of the first phase of descent, potential descent scenarios from the suggested LLOs to the Lunar surface will be analyzed in a second step. This analysis will be based on theoretical considerations. Nevertheless, fuel consumption, flight time, and possible landing sites will remain essential points of analysis in this phase as well.
In addition to the theoretical considerations regarding the descent trajectories, two case studies will be examined: the Orion capsule of NASA and the Starship of SpaceX. By using selected data, the feasibility of the previously analyzed descent trajectories with these two spacecraft will be evaluated. These two spacecraft have been chosen for this study due to the likelihood of their utilization by NASA for operational purposes in combination with the Gateway during the Artemis program.

Another objective of this work is to consider operational aspects, such as the stability of the communication link or potential eclipses. Here, the analyses will also be conducted with respect to the previously selected descent trajectories, thus examining their relevance for possible application in future space missions.
Finally, based on the analyses conducted earlier, recommendations will be made for the future selection of descent trajectories.

1.2 Approach

In order to achieve the objectives described in chapter 1.1, the open-source software SEMpy developed by the Space Advanced Concepts Laboratory (SacLab) of the renowned French university Institut Supérieur de l'Aéronautique et de l'Espace will be used.

However, since the software is primarily designed for the calculation of non-Keplerian orbits, some modifications need to be made for its use in this work. Specifically, the calculation and visualization of transfer trajectories between the Gateway's NRHO and the respective LLO need to be implemented.
Once this is done, the optimization of the transfer trajectories also needs to be adapted. The software already provides an example for optimizing the transfer between two Halo Orbits in terms of the required velocity changes. The free parameters for optimization in this case are the flight time and the start and end positions. These steps need to be performed for both the Circular Restricted 3-Body Problem (CR3BP) force model and the available ephemerides.
Then, the transfer trajectories for each combination of Gateway orbit and LLO can be computed and visualized. This allows for the analysis of the first section of descent trajectories to be performed. Following that, the theoretical description of descent from a LLO to the Lunar surface will be presented. Once both sections are adequately described, the focus will shift to the examination of the two case studies: the Orion capsule and the Starship. This analysis will be conducted using publicly available technical data for both systems.

The second part of the thesis focuses on the operational analysis of the selected transfer trajectories. To accomplish this, it is necessary to represent the transfer orbits in the OEM (Orbit Ephemeris Message) format. The OEM format is an internationally standardized format by the Consultative Committee for Space Data Systems (CCSDS). This is necessary to make the trajectories readable for a program developed by the German Aerospace Center (DLR). This program is capable of calculating the possible contact links with selected ground stations and identifying potential eclipse times during the transfer. Building upon the results obtained from this tool, the operational characteristics of the previously computed trajectories are then analyzed.

Finally, a summary of the previous analyses will be provided and the trajectories will be evaluated in terms of their suitability for the Artemis program.

Chapter 2

Background

As the main focus of this work is on the analysis of an optimal transfer trajectory between the orbit of the Gateway and a lower orbit around the Moon, the basics of dynamics in space are first illuminated.
It should be noted that the motion of bodies in space is mainly characterized by gravitational forces. These are mass-attracting forces that exist between all bodies with mass. The attractive force that two bodies exert on each other is given by equation 2.1 in magnitude [22].

$$F = G \cdot \frac{m_1 \cdot m_2}{r^2} \tag{2.1}$$

Here, G is the universal gravitational constant ($G = 6.67 \cdot 10^{-11} \frac{\mathrm{Nm}^2}{\mathrm{kg}^2}$). The variables m_1 and m_2 represent the masses of the two bodies, and r describes their distance. The inverse square dependence of the force on the distance indicates that the spread of the gravitational effect is a radiation law [22]. It can be observed that the attraction force increases as the masses increase and as the distance between the two masses decreases.

The consequence of these gravitational forces are the movements that all bodies in space perform. In general, it applies that all bodies in space are in motion at all times [1]. Ultimately, the mutual influence of all bodies results in the trajectories, which are referred to as orbits in technical language. These can assume any shape in space with a corresponding mass distribution and become increasingly complex the more bodies influence the test body.

As one of the most important resources in spaceflight is fuel, maneuvers to change an orbit are evaluated based on the change in velocity that the spacecraft must perform at a certain point in the orbit. This necessary change in velocity is referred to as Δv (*Delta V*) and is given in the unit of velocity ($[\frac{\mathrm{m}}{\mathrm{s}}]$).
Therefore, in the further course of this work, the proposed maneuvers for descent from the orbit of the Gateway to the surface of the Moon will be evaluated, among other factors, based on the required velocity demand.

2.1 Kepler orbits

If only two masses (central body and probe body) are considered for defining an orbit, the resulting orbits are Kepler orbits. To define a Kepler orbit precisely, certain assumptions need to be made. First, it is assumed that only the gravitational influence of the central body is significant for the motion of a body on the orbit. Furthermore, it is assumed that the mass of the central body is much greater than that of the body on the orbit. This implies that only the central body has an influence on the motion of the body, and the reverse is not true. Additionally, the gravitational field of the central body is assumed to be isotropic. This means that the field spreads uniformly in all spatial directions, and at equal distances from the central body, the same gravitational forces act throughout space. The central body is considered as a point mass [1].

Under these assumptions, an orbit around the central body is called a *Kepler orbit*. This name originates from the discoverer of this type of orbit, Johannes Kepler. A Kepler orbit is uniquely defined by six parameters (Kepler elements). These are presented in table 2.1.

Class	Parameter	Name
Shape of the orbit	a	Semi-major axis
	e	Eccentricity
Orientation in space	i	Inclination
	Ω	Right ascension of the ascending node (RAAN)
	ω	Argument of pericenter
Location on the orbit	ν/M	True/mean anomaly

Table 2.1: Table of parameters for defining a Kepler orbit [1]

The practical significance of the Kepler elements is illustrated in figures 2.1 and 2.2. The semi-major axis a and the eccentricity e describe the general shape of the orbit (see figure 2.1). When the eccentricity is 0, the orbit is circular. In this case, the semi-major axis corresponds to the radius of the orbit.

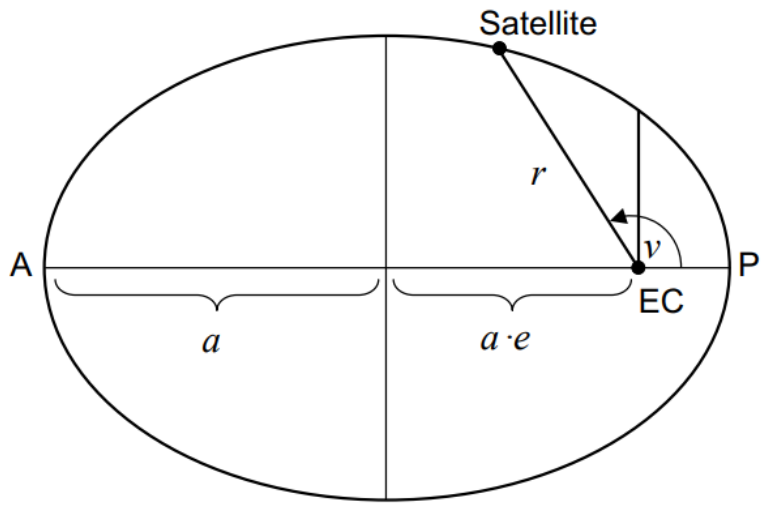

Figure 2.1: Sketch illustrating the Kepler elements: major axis 'a', eccentricity 'e', and true anomaly 'ν' for the unique definition of the orbit. [1]

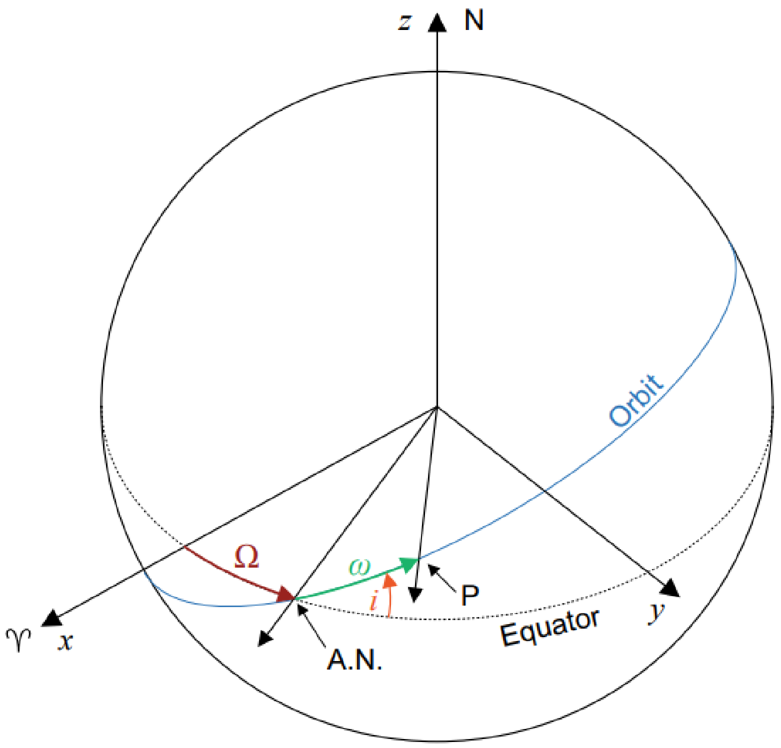

Figure 2.2: Sketch illustrating the Kepler elements: inclination 'i', right ascension of the ascending node 'Ω', and argument of pericenter 'ω' for the unique definition of the orbit. [1]

The additional Kepler elements, i, Ω, and ω, fundamentally describe the position and orientation of the orbit or orbital plane in space (see figure 2.2).
The inclination i, describes the angle between the equatorial plane of the central body and the orbital plane. The right ascension of the ascending node, Ω, describes the angle between the vector from the center of the central body to the vernal point ♈ (currently pointing towards the First Point of Aries) and the point where the spacecraft, traveling from south to north on the orbit, intersects the equatorial plane of the central body, called the ascending node [1]. The vernal point ♈ is the point where the Sun crosses the the celestial equator from south to north. It rotates with the precession of the Earth axis about 360° in roughly 25 900 years [23].
The third parameter for defining the position and orientation of the orbit in space is the argument of pericenter ω. This parameter represents the angle between the ascending node and the periapsis of the orbit, where the distance between the spacecraft on the orbit and the central body is at its minimum, thus the rotation of the orbit around the normal vector of its plane. In the case of a circular orbit, all points on the orbit are equidistant from the central body. Therefore, there is no uniquely defined argument of pericenter [1]. This applies to all the target orbits considered in this work.
The sixth Kepler element is the true anomaly ν. It describes the position of the spacecraft on the orbit and is defined as the angle between the radius vector to the pericenter and the radius vector to the spacecraft. In the case of a circular orbit, this parameter is also initially not uniquely defined. This is because, as mentioned earlier, there is no uniquely defined pericenter in this case [1].
The mean anomaly M is also an angle. It is used for orbits that are not circular. However, this angle is purely hypothetical. Similar to the true anomaly, the starting point of the angular measurement is the vector from the center body's origin to the orbit's pericenter. From there, the angle is measured to the position vector of the hypothetical position of the spacecraft. This hypothetical position is determined as a location on a circular orbit with the same period as the non-circular orbit, based on the elapsed orbital time.

2.2 Lambert Problem

The so-called Lambert problem can be traced back to the German mathematician, physicist, and astronomer Johann Heinrich Lambert (1728-1777) [2]. Fundamentally, this problem in astrodynamics involves finding a transfer trajectory between two orbits with a given flight duration [24].

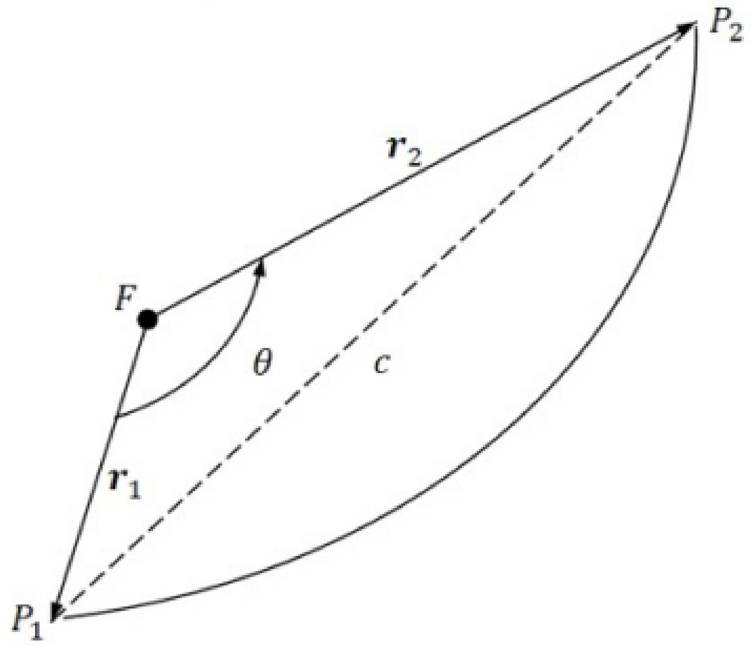

Figure 2.3: Sketch illustrating the definition of the Lambert problem [2]

Figure 2.3 shows a sketch for a more precise definition of the problem. Point F marks the central body around which the spacecraft's motion is to be performed. The vectors $\mathbf{r}_1$ and $\mathbf{r}_2$ describe the position vectors to the starting point (P_1) and ending point (P_2) of the transfer. The direct distance between the two points is indicated by the parameter c. The angle Θ corresponds to the angle between the two radius vectors $\mathbf{r}_1$ and $\mathbf{r}_2$ [2].

Other terms used to describe this astrodynamical problem include Gauss problem or Two-Body Orbital Boundary-Value Problem (TBOBVP) [2]. It should be noted that in the original formulation by Lambert and Gauss, only the gravitational influence of a central body was taken into account in the calculation of the transfer orbit. Furthermore, originally only transfer orbits that are part of a Keplerian orbit around the central body were considered. This is a consequence of treating the problem as a two-body problem [2].

The Lambert problem itself forms the basis of many modern astrodynamics problems and is therefore used in various practical applications, such as interception and rendezvous operations, ballistic missile trajectory planning, or the design of interplanetary transfer orbits [2]. Furthermore, it can occur that in the context of optimizations, not only one Lambert problem needs to be solved, but through iterations, numerous Lambert problems must be solved to find an optimal transfer orbit [25].
The extension of the original Lambert problem, where less than a complete orbit around the central body occurs on the transfer orbit, deals with the so-called multi-revolution solutions of the Lambert problem. In this case, on the transfer orbit representing the solution of the Lambert problem, more than one revolution around the central body takes place [25]. In the context of this work, both solutions of the Lambert problem with less than one revolution and solutions with more than one revolution around the central body are included in the investigations.

According to de la Torre Sangrà et al. [2], the general steps for solving the Lambert problem are as follows:

1. Calculation of the geometric parameters of the transfer.
2. Obtaining an initial value for the free parameter.
3. Iteration of the transfer time equation until convergence.
4. Calculation of the required velocity vectors.

To make these steps more tangible, the equation for the transfer time is provided under equation 2.2.

$$\sqrt{\mu} \cdot \Delta t = f(a, r_1 + r_2, c) \tag{2.2}$$

Here, μ represents the parameter of the central body ($\mu = G \cdot M$), where M is its mass. From equation 2.2, it follows that the flight time Δt is a function of the variables $a, r_1 + r_2, c$. Since the starting (r_1) and ending positions (r_2) are given, and thus the distance between them (c), the semi-major axis (a) represents the free parameter. This parameter is iteratively adjusted to achieve a continuous trajectory from the start to the destination point under other aspects [2].

In the first step, the geometrical aspects of the transfer are calculated. This involves determining the Kepler elements of the orbit, which the transfer trajectory corresponds to. Subsequently, the initial value for the free parameter is determined through input or computation. In the case of Gauss and Lambert, this was the semi-major axis of the orbit. In more sophisticated calculation methods, other parameterizations are now also used. In the third step, values for the free parameter are tested until the corresponding flight time eventually matches the initially given flight time within a certain error tolerance. Thus, the Lambert problem is solved. In the fourth step, the start and end maneuvers are calculated to both fly the calculated transfer with a predetermined initial velocity and then continue flying on the target orbit [2].

This approach is universally applicable and is implemented in various solution methods in different ways. However, the core of each step remains unchanged. Since Lagrange [26] and Gauss [27], numerous other scientists, researchers, and engineers have been studying the possibilities for solving the Lambert problem. Some of these approaches are listed below [2]:

- Universal Variables
- Calculation using the semimajor axis
- Calculation using the semi-latus rectum (p-iteration)
- Calculation using the eccentricity vector
- Calculation using Kustaanheimo-Stiefel (K-S) regularized variables

Hence, the Lambert problem is an important part of this work, as the main topic of the study is the analysis of various descent trajectories. In order to calculate the transfer trajectories between different orbits, the Lambert problem needs to be solved. Additionally, during the optimization of these transfer trajectories, numerous Lambert problems are solved through iterations to find the optimal descent trajectory.

Beyond the rough mathematical steps for solving the Lambert problem mentioned earlier, this work does not delve further into it. This is mainly due to the complexity of the solution methods. Gauss expressed this in his work "Theoria Motus Corporum Coelestium" [27] as follows:

„[T]his problem, to be considered among the most important in the theory of the motions of the heavenly bodies, is not so easily solved, since the expression of the time in terms of the elements is transcendental, and, moreover, very complicated.“

- Carl Friedrich Gauss

2.3 Circular Restricted 3-Body Problem

In the scope of this work, transfer orbits between the Gateway orbit and a Kepler Orbit (see chapter 2.1) or the Lunar surface are considered. Therefore, it is important to understand the fundamental dynamics on which the analyzed motions are based.
Many problems have to be considered with more than two bodies, e.g. in the Earth-Moon system, hence the so-called 3-body problem is of particular interest. This is because, in the scope of this work, both the gravitational influence of the Earth and the gravitational influence of the Moon on the spacecraft are taken into account. The 3-body problem itself has been studied by mathematicians for over 200 years due to its mathematical interest. For the 3-body problem, analytical solutions can only be found for special cases, which leads to the usage of approximations for practical purposes. [28].

One of these simplifications is the Restricted 3-Body Problem, which can be applied without significant loss of accuracy. The most general form of the Restricted 3-Body Problem is the Elliptical Restricted 3-Body Problem (ER3BP), where the motion of the central bodies is assumed to be elliptical. For the analyses conducted in the following chapters, an additional simplification of the ER3BP has been applied. In this simplification, the orbits of the central bodies are not only assumed to be elliptical but even circular. The dynamics of this further simplified model is referred to as the CR3BP [28].

To define the CR3BP, as in the case of Kepler orbits (see chapter 2.1), several assumptions are made:

- There are two primary masses, and the mass of the tertiary object is extremely small in comparison to the two primaries
- The two primary masses orbit around their common barycenter on circular paths [29]
- The two primary masses are point masses [29]

The coordinate system used to describe the motion of the spacecraft is called synodic reference frame (see figure 2.4). This coordinate system has its origin at the barycenter of the two central bodies and rotates at a constant angular rate ω, which corresponds to the rotation of the two central bodies around each other [29]. The x-axis points radially from the barycenter towards the Moon, the z-axis points in the direction of the angular momentum vector, and the y-axis completes the right-handed coordinate system [28].

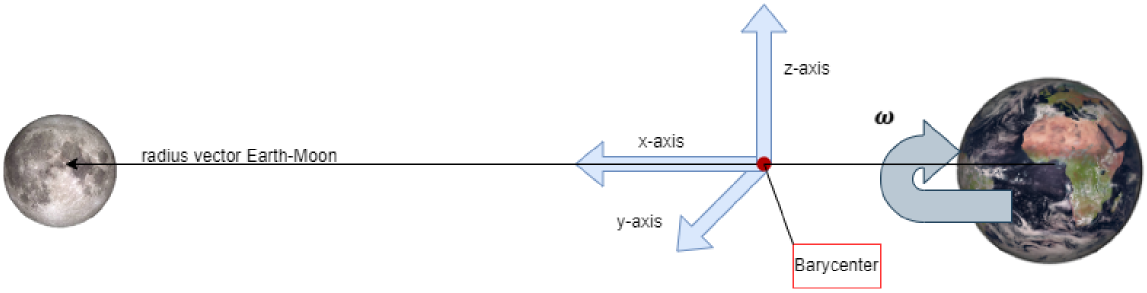

Figure 2.4: Sketch illustrating the synodic reference frame [3][4]

The CR3BP has five points in space where the gravitational attractions of the Earth and the Moon and the centrifugal forces balance out, rendering the third body of the CR3BP (spacecraft) force-free. These points are known as Lagrange points. Figure 2.5 depicts the location of the Lagrange points with respect to the positions of the Earth and the Moon. The collinear points L1, L2, and L3 lie on the line passing through the centers of mass of the Earth and the Moon. The equilibrium points L4 and L5 form equilateral triangles with the two central bodies [29].

However, in the subsequent course of the work, only the two points L1 and L2 will be of interest, as they allow to define special kind of non-Keplerian orbits around them. (see chapter 2.6).

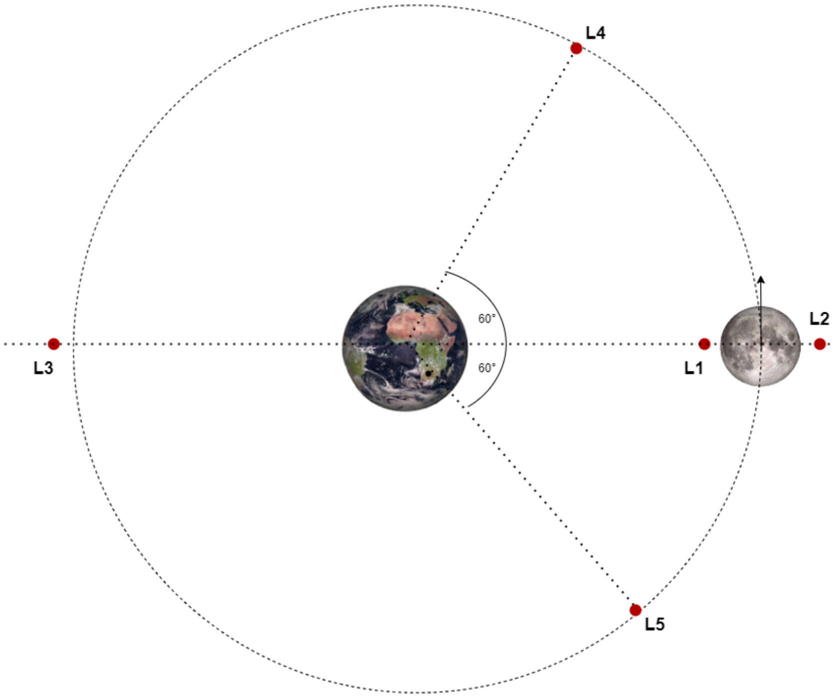

Figure 2.5: Sketch illustrating the positions of the Lagrange points in the CR3BP [3][4]

2.4 Ephemerides

As bodies of all kinds move in space at all times, the gravitational forces they exert on each other also constantly change. This is due to the changing distances between the bodies caused by their continuous motion. This can be clearly seen in equation 2.1, as the distance between the two bodies is involved in the calculation of the gravitational force. Now, it is true that this behavior also applies to all bodies in our solar system. Therefore, the constant change in mutual gravitational forces also applies to the Earth and the Moon, both of which play a central role in the context of this work. The result of these motions is a continuously changing gravitational field, which eventually leads to the fact that the orbit of a body never exactly repeats itself. Accordingly, the assumption made in chapter 2.3 that the Earth and the Moon rotate around each other on repeating circular orbits is not correct in reality. In reality, an orbit is never closed and never repeats itself in the same way [30].
In order to incorporate this into the calculation of the gravitational forces acting on a spacecraft or any other body, it is necessary to be able to predict the position of each body in space. This is done using numerical methods and countless iterations and adjustments [30].
In order to perform these iterations and improve the calculations, ephemerides are used. The term ephemerides originally referred to a table of positions of celestial bodies at a specific time. Nowadays, the term ephemerides refers to more modern methods such as polynomial and time-continuous data files [30].

When referring to ephemerides or ephemeris models in the context of this work, it means the calculation of the respective orbit or trajectory uses precisely determined positions and resulting gravitational forces of the relevant central bodies.
Since the solar system bodies' positions depend on the chosen epoch, a consistent start epoch for the calculations was chosen. Therefore, a consistent start epoch of June 1, 2020, 12:00:00.000 (Universal Time Coordinated (UTC)) was used in this work for the calculations.

2.5 Halo Orbits

The discovery of Halo Orbits dates back to the 18th century, credited to the mathematicians Euler (1767) and Lagrange (1772). Euler and Lagrange discovered the existence of equilibrium points in a force field composed of two central bodies [31]. These points later became known as Lagrange points (refer to chapter 2.3).

Although the existence of these points has been known since then, their surroundings were not explored in terms of the existence of possible orbits or other applications. This changed in the 1950s when Arthur C. Clarke proposed the L2 point of the Earth-Moon system (see figure 2.5) as a location for a relay system for potential colonization of the far side of the Moon. Approximately 15 years later, Robert Farquhar discovered trajectories around the L2 point that allow positioning a communication satellite to ensure continuous connectivity between Earth and the far side of the Moon [31].

Robert Farquhar named these types of trajectories *Halo Orbits* because they appear like halos around the Moon when viewed from the Earth [31]. However, Halo Orbits themselves are not perfectly round and planar, as one would expect from a halo. Their shape is best described by that of a potato chip. Figure 2.6 shows a series of Halo Orbits of the Earth-Moon system. It includes orbits around the Lagrange point L_1 (see figure 2.5) (purple and blue) as well as orbits around the L_2 point (see figure 2.5) (green, red, and yellow).

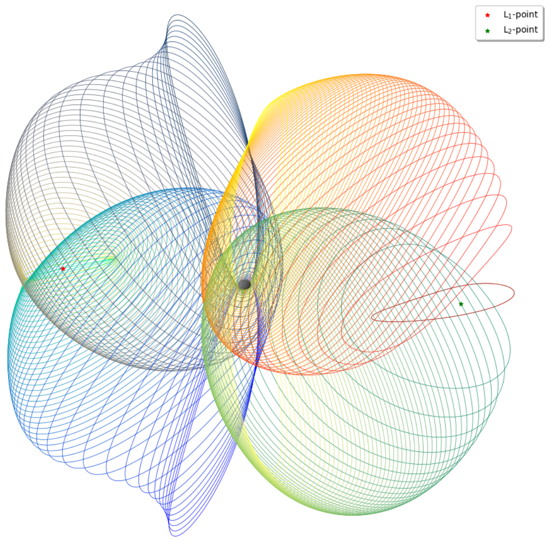

Figure 2.6: Graph depicting some example Halo Orbits around the L_1 and L_2 points of the Earth-Moon system, generated using an example script from the SEMpy software [5]

In the late 1960s and early 1970s, numerous engineers and scientists were involved in various projects related to manned Lunar missions due to the Apollo program of NASA. This also advanced the exploration of Halo Orbits in the Earth-Moon system and other 3-body mass systems [31].
In the following years, various space missions were carried out that made use of these Halo Orbits. Two examples of such missions are the International Sun-Earth Explorer (ISEE) program, as well as the Solar and Heliospheric Observatory (SOHO) mission [31]. Both missions were conducted jointly by NASA and ESA.

Generally, Halo Orbits refer to orbits defined in relation to the equilibrium points of a gravitational field. It doesn't matter exactly which masses (e.g., Sun, Earth, Moon) are involved. Due to the balancing gravitational forces at the equilibrium points and the resulting forces in their vicinity, Halo Orbits are closed or nearly closed trajectories, along which spacecraft can continuously move without drifting significantly away from the central bodies.
Figure 2.7 illustrates some of these trajectories. These are the southern Halo Orbits around the L_2 point of the Earth-Moon system. They correspond to the same trajectories depicted in green in figure 2.6.

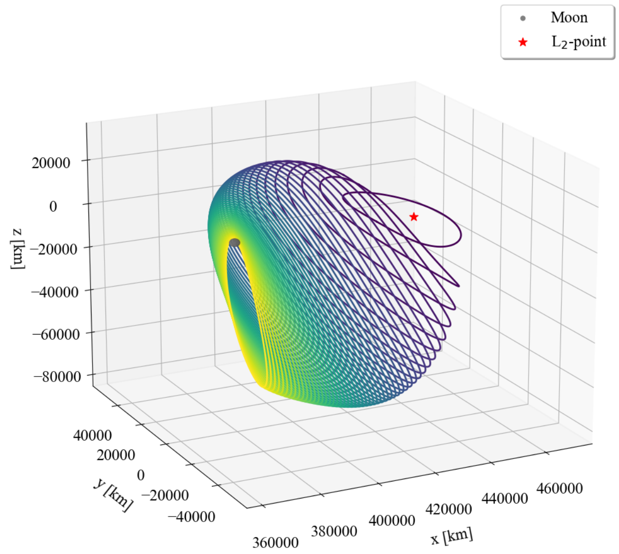

Figure 2.7: Graph depicting several exemplary southern Halo Orbits around the L_2 point of the Earth-Moon system, generated using a sample script from the SEMpy software [5]. These orbits represent a zoomed-in view of the green trajectories shown in figure 2.6

2.6 Near Rectilinear Halo Orbits

The orbit currently selected by NASA for the Gateway is a specific type of Halo Orbit, known as a NRHO. While NRHOs are a type of Halo Orbit, they possess certain characteristics that distinguish them from other Halo Orbits [7]. Figure 2.8 illustrates the southern Halo Orbits around the L_2 point of the Earth-Moon system, with the white markers indicating the NRHOs that define the region within the southern L_2 Earth-Moon Halo Orbits [6].

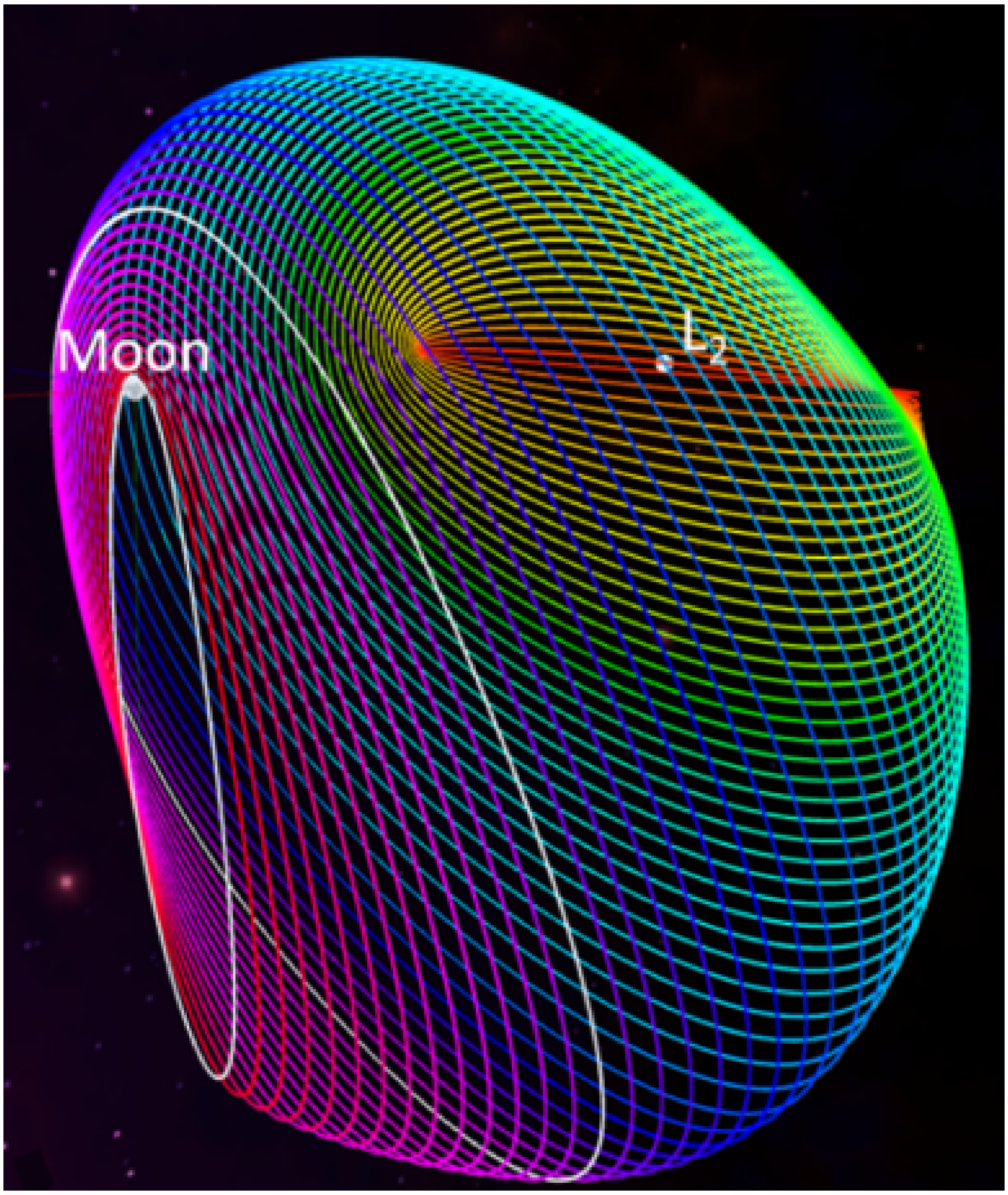

Figure 2.8: Graph depicting some example southern Halo Orbits around the L_2 point of the Earth-Moon system, with the boundaries of the NRHOs highlighted in white [6]

An important characteristic that distinguishes a NRHO from other Halo Orbits is the low altitude of the orbit's pericenter over one of the Moon's poles. This is particularly useful for missions targeting the Lunar surface, as it requires less velocity change for descent [7]. The minimum radius of the orbit at the pericenter is also a defining feature of an NRHO [32].
Due to the low pericenter, short transfer times of approximately half a day are achievable, which is especially relevant for manned missions to the Lunar surface [7].
In the case of the Moon, the low pericenter of the NRHO is accompanied by a high apocenter over the opposite pole. This can be particularly useful for achieving long communication windows between the orbit (Gateway) and a potential landing site on the Lunar south pole [7].

Another characteristic of NRHOs is their periodicity in the CR3BP. When the CR3BP is used as the model for gravitational forces, NRHOs are closed trajectories that repeat continuously. However, this changes when more accurate force models, such as ephemerides, are applied. In this case, NRHOs are no longer periodic but rather quasi-periodic [32]. This means that while they exhibit periodicity in their shape, they do not form closed trajectories.
In addition to periodicity, stability is an important property of NRHOs. Due to their neutral stability characteristic, NRHOs experience only small deviations from the nominal orbit during operation. This results in low fuel costs to maintain a spacecraft in orbit [7]. Furthermore, NRHOs remain relatively fixed in space with respect to the Earth-Moon plane. They also rotate at the same rate as the Moon orbits the Earth and rotates around its own axis [33]. This has the advantage that the normal vector of an imaginary orbital plane always points towards Earth, allowing continuous communication with ground stations on Earth.

Finally, it is worth mentioning the possibility of delivering cargo to an NRHO from Earth using a Four-Body Ballistic Lunar Transfer (BLT). Although this method requires a long flight time, thus making it problematic for manned spaceflight, this is irrelevant for unmanned spacecraft used for cargo transportation. The major advantage of this approach in supplying the Gateway with cargo lies in the low fuel requirement for BLT transfers [7].

To illustrate the previously described characteristics, figure 2.9 shows some southern L_1 and L_2 NRHOs of the Earth-Moon system.
The low pericenter and the very high apocenter can be seen clearly. In addition, the periodicity of the orbits in CR3BP can be seen from the closed orbits. The orbits in the right part of the figure are orbits around the L_2 point. The orbits in the left part are the orbits defined with respect to the L_1 point.

Figure 2.9: Graph of some exemplary southern NRHO orbits around the L_1 and L_2 points of the Earth-Moon system. [6]

Chapter 3

Orbital mechanical analysis of the descent trajectory

In the context of the orbital mechanics analysis of the descent from the Gateway orbit to the Lunar surface, as described in chapters 1.1 and 1.2, the first step is to examine the descent from the Gateway orbit to a LLO.
To do this, the specific orbits of the Gateway and three selected LLO will be explained, which will then be used as a basis for the analyses in this work.

3.1 Orbit of the Gateway

As described in the previous chapters 2.5 and 2.6, the Gateway orbit is generally a Halo orbit and specifically a NRHO. The general advantages of this type of orbit have also been explained in chapter 2.6.
As a result of various considerations, NASA has chosen a specific NRHO of the L_2 Southern Family as the precise orbit for the Gateway. Furthermore, a 9:2 Lunar Synodic Resonance (LSR) has been specified for the orbital period. This means that a spacecraft completes 9 orbits while the Moon completes 2 orbits around the Earth [7].

Generally, the southern NRHOs were chosen for the operation of the Gateway due to their lower propellant requirements for a spacecraft returning from the Gateway to Earth. This is because a splashdown in the northern hemisphere is specified as the return location to Earth, which is driven by geopolitical considerations [7].
Since the orbits of the L_2 Southern Family provide better visibility of the far side of the Moon, enabling improved communication in that area, they were preferred over the orbits of the L_1 Southern Family in the selection process [7].

Additionally, the NRHOs of the L_2 Southern Family exhibit a more stable characteristic in the considered region. This results in spacecraft or the Gateway requiring less propellant to maintain their orbit compared to spacecraft on comparable NRHOs of the L_1 Southern Family [7].

An orbit with a LSR period was chosen as it provides the opportunity to avoid eclipses, especially by the Earth [7]. This is particularly relevant because an eclipse leads to significant temperature fluctuations with very low temperatures and renders solar cell power production impossible. Only the eclipses caused by the Earth are relevant, as the eclipses caused by the Moon do not have the necessary duration to excessively strain the existing power system of the Gateway.
The significant temperature differences during solar exposure and during an eclipse would pose a major challenge for the thermal system of the Gateway. This is not only due to the high and low temperatures themselves but also because of the rapid temperature fluctuations occurring within a very short period of time. This would subject the materials of the Gateway to severe stress.
The temporary power outage during an eclipse would also impose high demands on the power system of the Gateway. Even during the eclipse, the power supply, including necessary redundancies, would need to be ensured, requiring sufficient storage capacities. While these capacities are already available for safety reasons, they would need to be expanded. This would ultimately complicate the overall system of the Gateway and make the development, construction, and operation more costly. In figure 3.1, the eclipses caused by the Earth and the Moon until 2035, as calculated by NASA, are shown, which a spacecraft on the specified orbit would experience.

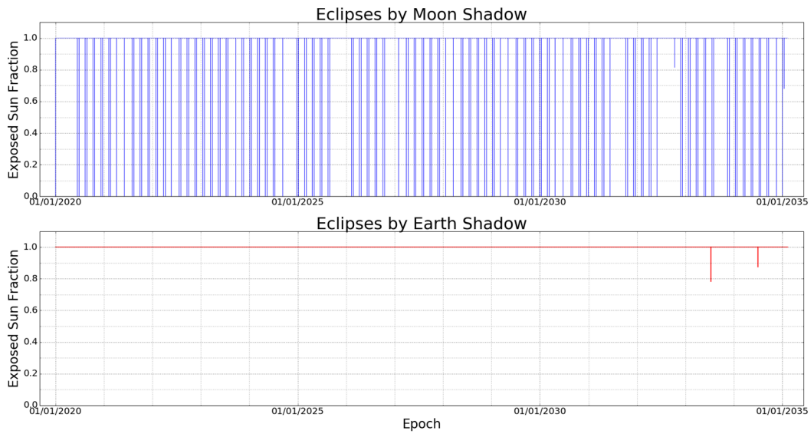

Figure 3.1: Visualization of the eclipses that a spacecraft on the Gateway's chosen orbit (L_2 Southern NRHO) experiences within a timeframe until 2035, as determined by NASA [7]

As shown in the figure, eclipses caused by the Moon occur relatively frequently. However, the more relevant eclipses caused by the Earth are completely absent except for two events at the end of the timeframe until 2035. These two events are expected to be mitigated through previous maneuvers, ensuring that no eclipses caused by the Earth occur within the specified timeframe.

The specific orbit selected by NASA for the operation of the Gateway is a NRHO with a pericenter radius ranging from 3196 km to 3557 km (average of 3366 km). The variations are due to the quasi-periodicity of the orbit. The period of this orbit averages approximately 6.562 days [7].
For the analyses to be conducted in the following sections, an NRHO with a pericenter radius of 3250 km was chosen. This selection was made to enable comparison of the results with the work of Whitley et al. [34]. Figure 3.3 depict the chosen orbit. These visualizations were created using the SEMpy software, which was also utilized for the subsequent analyses.

In addition to SEMpy, the FreeFlyer software of the company a.i.solutions was used. The software is used for the design, analysis and execution of space missions. In the context of the thesis, the tool was used to provide independent validation of the results calculated with SEMpy. For this purpose, figure 3.2 shows an exemplary graph of the selected orbit of the Gateway.

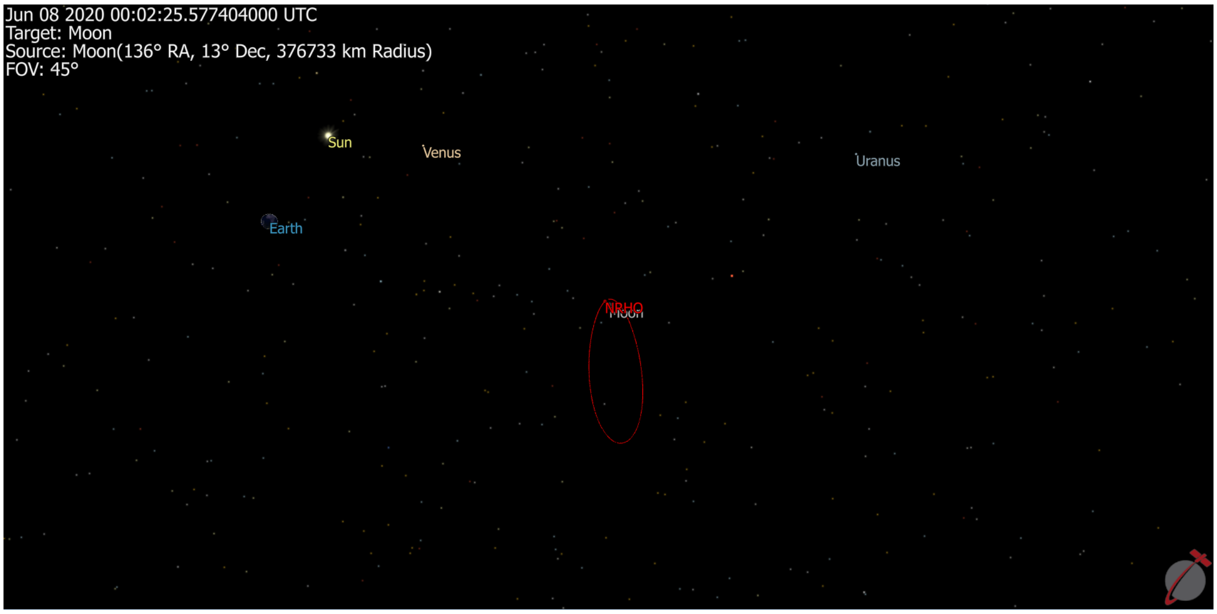

Figure 3.2: L_2 southern NRHO with a pericenter radius of 3250km used for the analyses of the work, generated with FreeFlyer

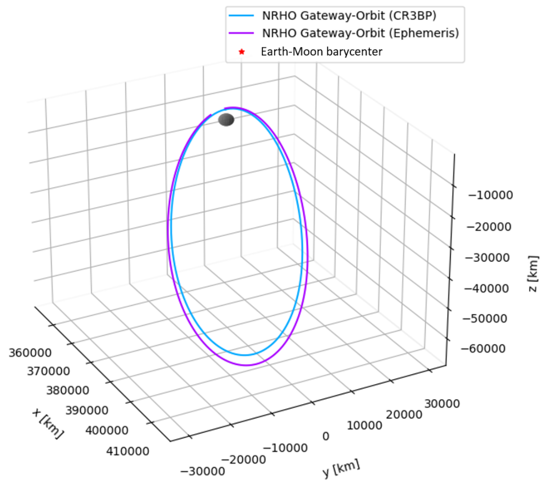

(a) Micro 3D-view

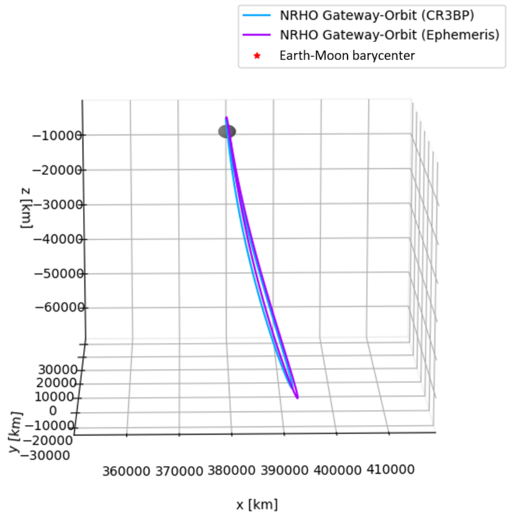

(b) View of x-z-plane

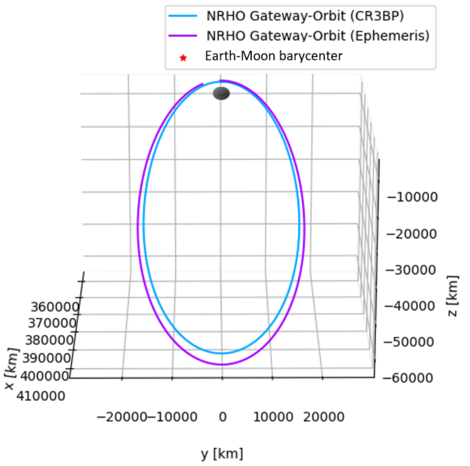

(c) View of y-z-plane

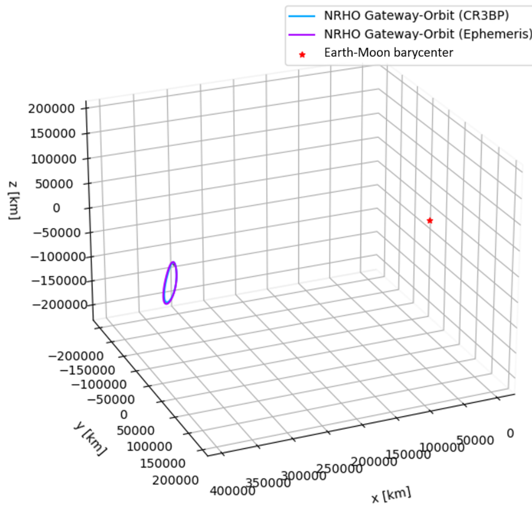

(d) Macro 3D-view

Figure 3.3: Figures (a), (b) and (c) show the Gateway's L_2 southern NRHO with a pericenter radius of 3250 km, used for the analyses in this work, generated using SEMpy in the CR3BP and ephemeris force model from different perspectives. Figure (d) shows the Earth-Moon barycenter as well.

3.2 Low Lunar Orbits

After describing the Gateway orbit (initial orbit) in the previous chapter 3.1, we will now examine the LLOs that serve as target orbits for the first phase of the descent analysis.
A total of three representative circular Kepler orbits were chosen for the LLO. They all have an altitude of 100 km above the Lunar surface, when considering a mean radius of the Moon of 1737 km. Since the Moon does not have an atmosphere, there are no atmospheric drag losses at this low altitude, making the orbits assumed to be stable. The three selected orbits cover all cases of circular Kepler orbits with an altitude of 100 km in the sense that all other possible orbits with their Kepler elements lie between the values of the selected orbits. Therefore, it is expected that the results for these orbits will fall within the range of the achieved results for the selected orbits.
In table 3.1, the Kepler elements of the 3 selected LLOs are listed. LLO 1 is a polar orbit that is approximately coplanar with the selected NRHO. It can be only approximately coplanar because the NRHO itself is not planar (see figure 3.3 (b)). LLO 2 is also a polar orbit, but the ascending node is rotated by 90 degrees compared to LLO 1. The third orbit, LLO 3, is an equatorial orbit.

Orbit	a	e	i	Ω	ω	ν
LLO 1	1837km	0.0	$-\frac{\pi}{2}$	$\frac{\pi}{2}$	0.0	0.0
LLO 2	1837km	0.0	$-\frac{\pi}{2}$	0.0	0.0	0.0
LLO 3	1837km	0.0	0.0	0.0	0.0	0.0

Table 3.1: Table of Kepler elements for the selected LLOs used in the analyses

In figure 3.4, LLO 1 is depicted. In figure 3.5, LLO 2 is shown, and in figure 3.6, LLO 3 is displayed. All graphics were created using SEMpy software.
For the sake of clarity, a macro and micro view were created for each LLO. Additionally, the entire orbit, including the portion obscured by the Moon, is shown.

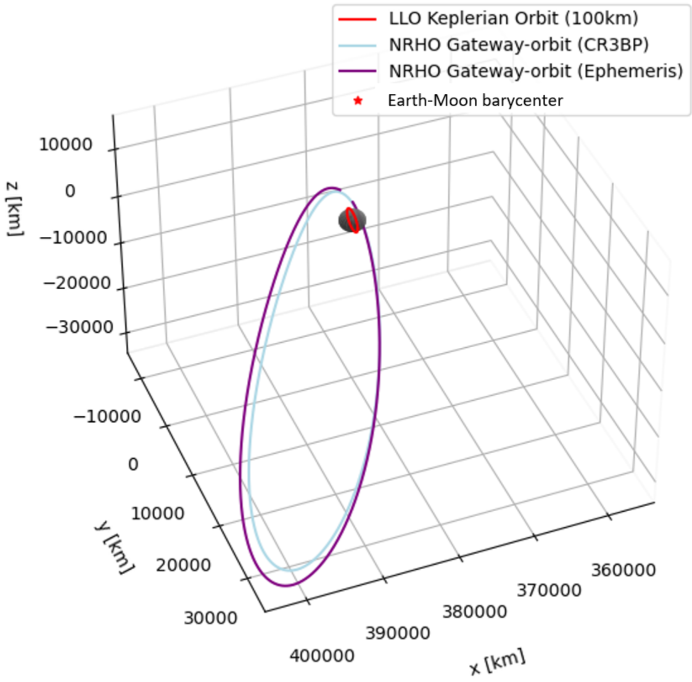

(a) Macro View

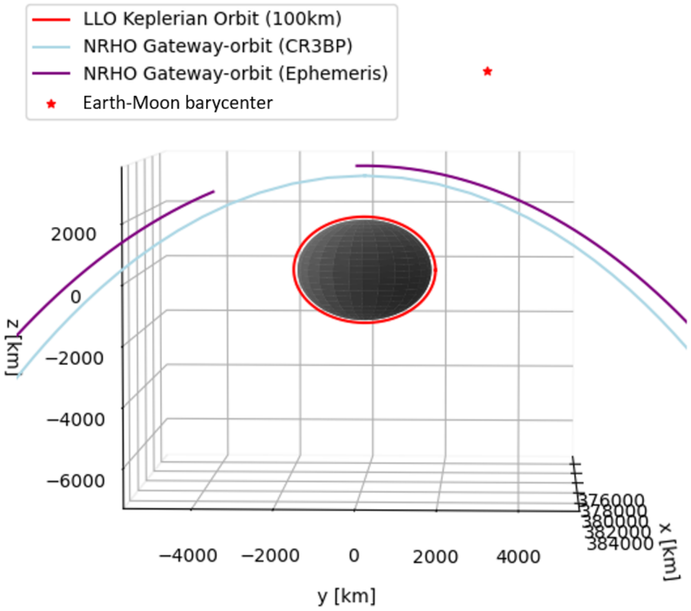

(b) Micro view

Figure 3.4: LLO 1 with a semi-major axis of 1837 km and the orbit of the NRHO (see chapter 3.1) - generated with SEMpy

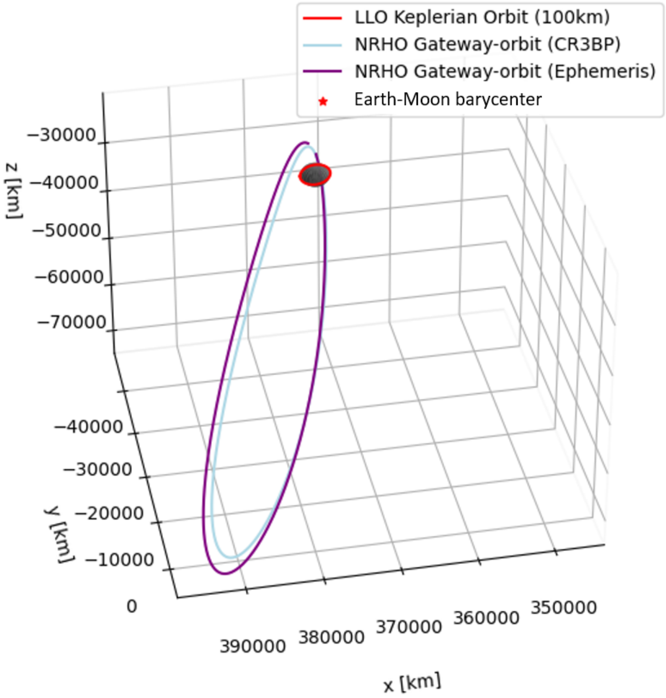

(a) Macro View

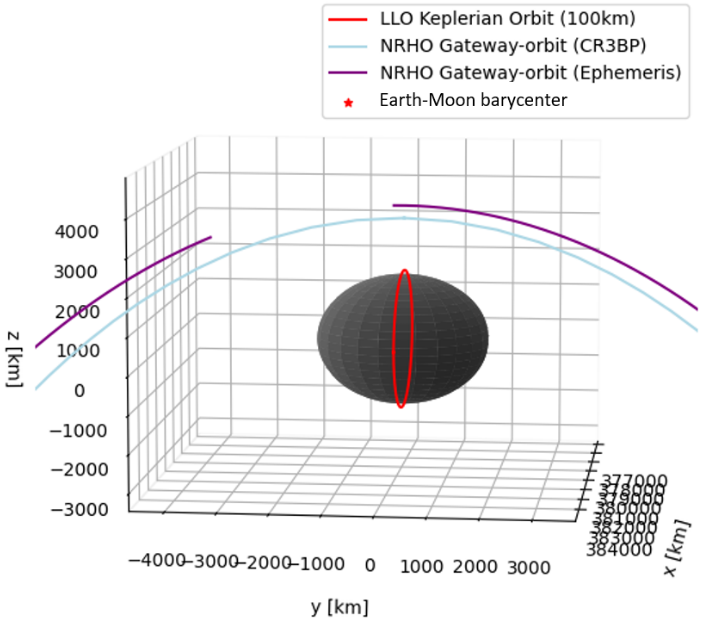

(b) Micro view

Figure 3.5: LLO 2 with a semi-major axis of 1837 km and the orbit of the NRHO (see chapter 3.1) - generated with SEMpy

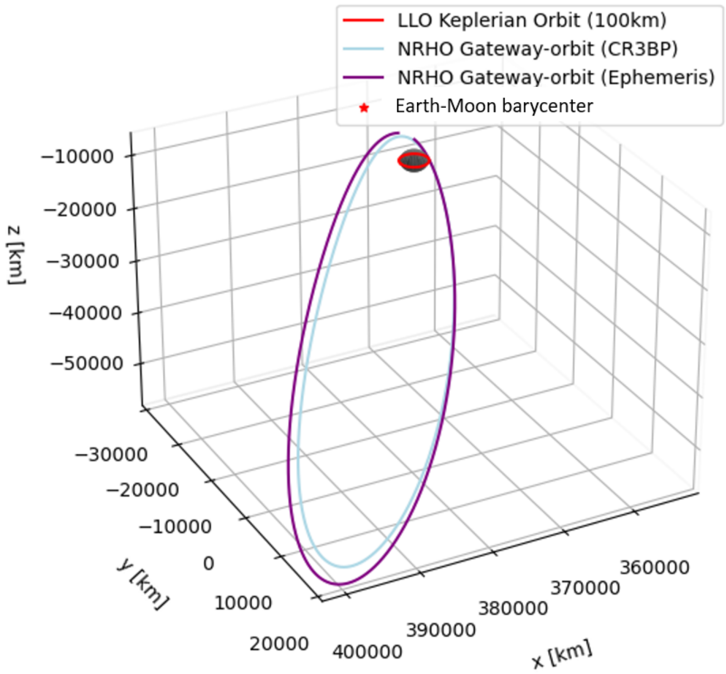

(a) Macro View

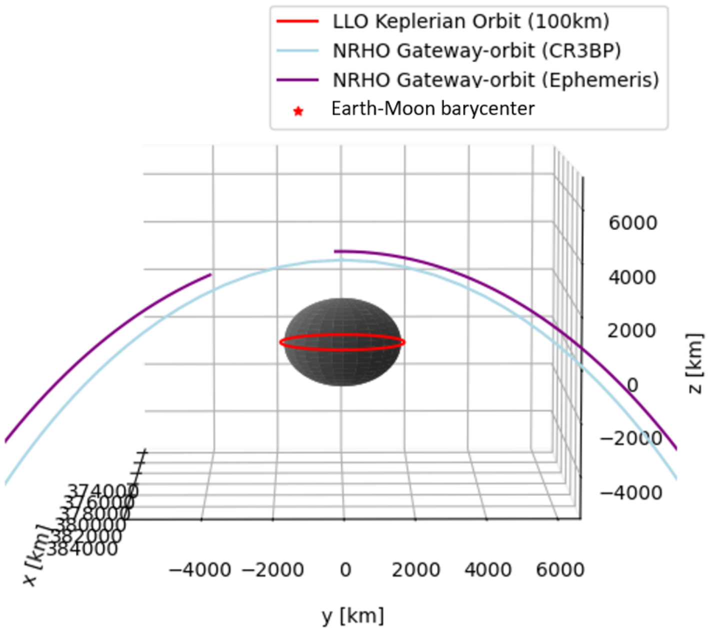

(b) Micro view

Figure 3.6: LLO 3 with a semi-major axis of 1837 km and the orbit of the NRHO (see chapter 3.1) - generated with SEMpy

To provide an overview and comparison, in the following figure 3.7 all three LLOs are depicted in a single graph. The orbit of the Gateway is visible in the background, both in the CR3BP and ephemeris models.

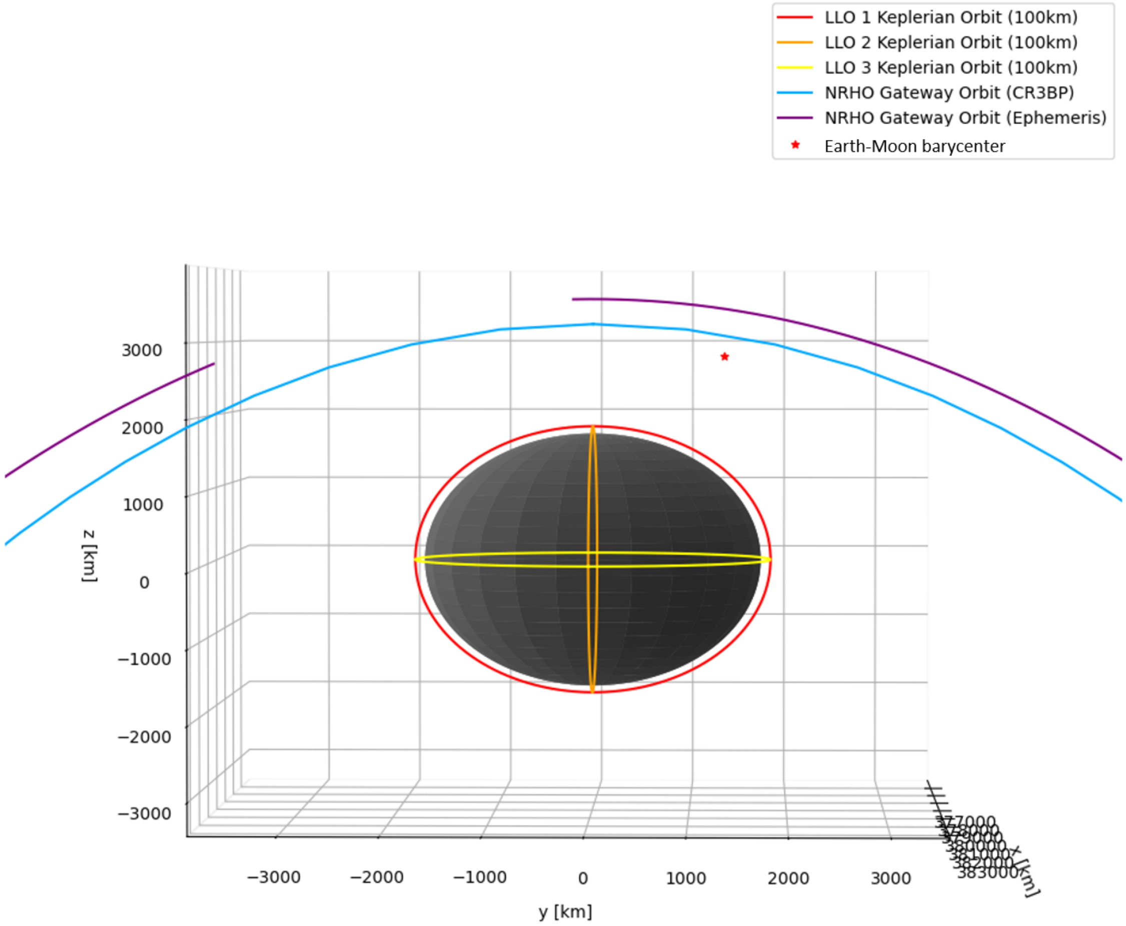

Figure 3.7: Visualization of all three LLOs with the Gateway orbit in the background (CR3BP and ephemerides), generated using SEMpy (parts of the LLOs 2 and 3 behind the moon are shown as well)

3.3 SEMpy

As described in the previous chapter 1.2, the Python3 library SEMpy [5] was used to conduct the analyses of the different descent trajectories. SEMpy is an open-source software developed by the Space Advanced Concepts Laboratory (SacLab) at the renowned French university Institut Supérieur de l'Aéronautique et de l'Espace. The acronym SEMpy stands for the software's focus on computing the gravitational field with the central bodies **S**un, **E**arth, and **M**oon, and the code is written in the programming language **Py**thon. The software provides advanced astrodynamics tools, including mission analysis for missions moving on non-Keplerian orbits. This includes the force model of the CR3BP (see chapter 2.3) and the more accurate ephemeris model. However, the library also supports many other applications, such as rendezvous missions or mission analysis of spacecraft with low-thrust propulsion systems [5].

The library is available at the following link: *https://gitlab.isae-supaero.fr/sempy*, on the profile of Institut Supérieur de l'Aéronautique et de l'Espace on the publicly accessible GitLab platform. Included in the software are several exemplary scripts that aim to facilitate the introduction and use of the codes. These include:

- Examples for generating Halo Orbit families
- Examples for calculating Halo Orbits using the ephemeris model
- Examples for solving the Lambert problem related to Halo Orbits
- Examples for generating general Halo Orbit data in the CR3BP
- Examples for visualization

Furthermore, there is also an exemplary code for generating Kepler Orbits in the context of low-thrust trajectories. The available examples served as a starting point for the further development of the necessary scripts and were supplemented with the required functionalities.
However, there were some difficulties due to the fact that SEMpy is primarily focused on the calculation of non-Kepler orbits. Since the analyses in the first section of the descent evaluate a descent from the Gateway's NRHO to LLOs, which are Kepler orbits, it was necessary to extend the functionalities of the Halo Orbits to include similar functionalities for the Kepler Orbits.

To achieve this, the following scripts were developed as part of this work on the basis of given examples provided by SEMpy. It resulted in a duality because scripts had to be created for both the CR3BP and the calculation with the ephemerides. The scripts are very similar except for some adjustments regarding the force model.

- **Script for computing and visualizing a transfer in the CR3BP**
- **Script for computing and visualizing a transfer with ephemerides**

- Script with functionalities for solving Lambert's problems in the CR3BP
- Script with functionalities for solving Lambert's problems with ephemerides

- Script for optimizing transfer trajectories in the CR3BP
- Script for optimizing transfer trajectories with ephemerides

- Script for storing computed orbits and transfer trajectories of the CR3BP in OEM format
- Script for storing computed orbits and transfer trajectories of ephemerides in OEM format

- Script for computing the state vector in the respective force model
- Script for generating the orbit of the Gateway NRHO based on ephemerides
- Script for sampling the range of values of start and end positions to find the best values for the velocity requirements of the transfer

The two bold scripts were used to compute the results for the analysis of the descent trajectory. The remaining listed scripts include the key functionalities needed in the two main scripts.

The flowcharts of the two main scripts are presented in figures 3.8 and 3.9 to provide a visual representation of the program flow.

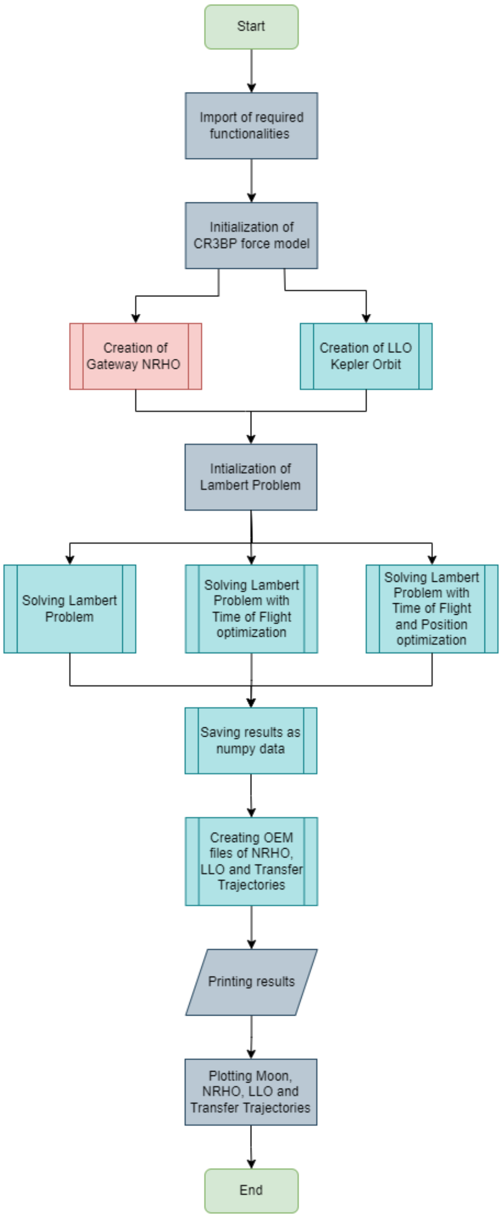

Figure 3.8: Program flowchart for calculating and generating the transfer trajectories from the NRHO of the Gateway to an LLO in the CR3BP force model

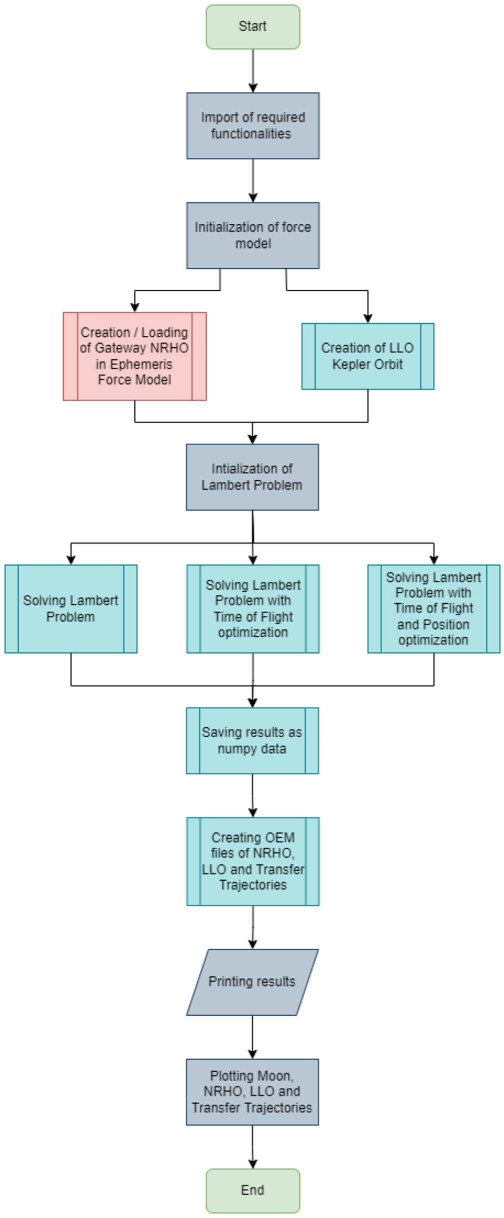

Figure 3.9: Program flowchart for calculating and generating the transfer trajectories from the NRHO of the Gateway to an LLO in the ephemeris force model

As evident from the comparison of figures 3.8 and 3.9, the two scripts are similar with one important difference. The step that distinguishes the two scripts is the calculation of the Gateway's orbit, highlighted in red. One script performs this calculation using the CR3BP model, while the other script utilizes the ephemerides. Consequently, there are minor variations in the subsequent steps of the scripts, which are not specifically highlighted in the flowcharts of the two figures.

Nonetheless, both calculations follow a similar process, so we will focus on the specific details of the calculations in the CR3BP in the following discussion (see figure 3.8).

The script can be executed either from the terminal or from an integrated development environment (IDE). In the case of this work, the PyCharm IDE from the Czech company JetBrains was used. After importing all the necessary libraries, classes, and functionalities, including those from the listed scripts, the CR3BP force model is initialized. This involves defining the central bodies to be included in the calculations, as well as other characteristic parameters. Subsequently, the Gateway's orbit in the CR3BP and the target Kepler orbit are calculated.

Next, the parameters of the Lambert problem are determined. These include the transfer time and the start and end positions on the initial and target orbits, respectively. During the optimization process, these values are used as initial values. Additionally, other parameters, such as the number of revolutions around the central bodies allowed during the transfer, can also be specified.
Next, the Lambert problems are solved using three different approaches. In the first case, the start and end positions, as well as the flight time, are pre-determined. In the second case, only the start and end positions are fixed, and the flight time can be dynamically adjusted during the calculation. The third case allows for dynamic determination of all three parameters. In the second and third cases, optimization is performed while solving the equations for the Lambert problem. This optimization is carried out using the PyGMO Python library, specifically utilizing the local optimization algorithm called *Cobyla*. This algorithm was chosen because an example of optimization with various algorithms was already available in SEMpy, and it produced the best results in the analyses. However, it should be noted that this is a local optimization algorithm.

Once all three Lambert problems have been solved and the optimization process is completed, the resulting transfer trajectories are saved in the *numpy* data format. Additionally, text files in the OEM format are generated for the results, the start and the target orbits. As described in chapter 1.2, these transfer trajectories in the OEM format are needed for further operational analyses in chapter 4.

Finally, the flight time and the magnitudes of the impulsive velocity changes for each transfer are displayed in the command line, and graphs of the transfer with the start and target orbits are generated. These graphs serve for visualization in the context of the work and for visually confirming the correct calculation of the obtained results.

To elaborate on the difference between the two scripts, let's discuss the calculation of the Gateway's orbit phenomenologically. Firstly, it should be noted that the Gateway's NRHO is calculated in both the CR3BP and the ephemeris model using a method called *Differential Correction*. To describe this method in general terms, it can be said that a set of conditions in mathematical equations is adjusted until a set of criteria is met within a sufficient tolerance. Within this method, two subcategories are distinguished: *Single-Shooting Differential Correction* and *Multiple-Shooting Differential Correction* [8].

The Single-Shooting Differential Correction method starts with an initial position that remains unchanged and a target position that needs to be achieved. During the calculations, the conditions that must also be taken into account are varied until the calculations converge, and the initial and target positions are achieved through suitable intermediate states [8].
To illustrate this theoretical explanation with an example, let's consider the maneuver planning of a spacecraft that needs to fly from a certain initial position to a target point. The spacecraft has a fixed initial state, namely its position. The initial velocity is variable as it can be adjusted through engine ignition, and in the calculation, it is considered as a free condition. The same applies to the target state. The target position is predefined, but the velocity at which the spacecraft arrives at the target position is freely adjustable and can also be modified through engine ignition if necessary. Another free condition is the flight time, as it is initially not determined how long the spacecraft should fly from the initial to the target state. In the calculations of the Single-Shooting method, the initial and target velocities and the flight time are adjusted until a trajectory is found that passes through the initial and target positions [8].

In figure 3.10, the corresponding graph is shown. The solid line represents the state before the calculation, and the dashed line represents the result of the calculation. $\mathrm{X}(t_0)$ describes the initial state (position and velocity) that exists before the calculation. $\hat{\mathrm{X}}(\hat{\mathrm{t}}_0)$ describes the initial state that is given as the result of the Single-Shooting procedure. $\mathrm{X}(t_0)$ and $\hat{\mathrm{X}}(\hat{\mathrm{t}}_0)$ differ only in their velocity vectors; the position is the same. The original flight time T is changed to the value $\hat{\mathrm{T}}$ through the calculation. The two final states $\mathrm{X}(t_f)$ and $\hat{\mathrm{X}}(\hat{\mathrm{t}}_f)$ differ in both position and velocity. The final position is predetermined within the calculation, and the velocities differ due to the different flight paths [8]. In the context of this work, the Single-Shooting Differential Correction is used by SEMpy, among other things, in the Multiple-Shooting procedure to calculate the NRHOs in the CR3BP as well as with the ephemeris.

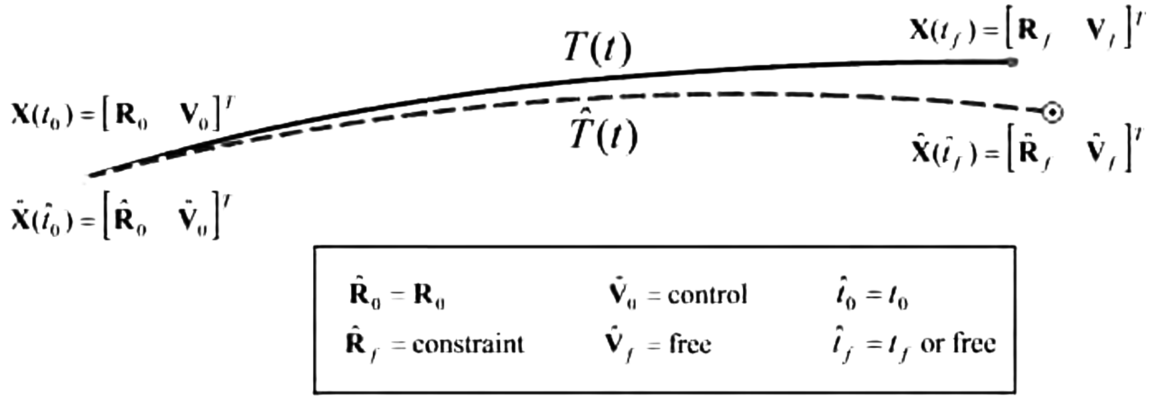

Figure 3.10: Figure illustrating the exemplary explanation of the Single-Shooting Differential Correction method [8]

The Multiple-Shooting Differential Correction method is based on the Single-Shooting method. The Multiple-Shooting approach uses multiple states and simultaneously adjusts them using the Single-Shooting method to satisfy a set of boundary conditions. This is particularly useful for long-distance flights or orbits, as it subdivides the entire trajectory into smaller segments, reducing the error that would occur in the calculation using the Single-Shooting method compared to a real trajectory [8].
SEMpy utilizes this method to create a continuous trajectory in the CR3BP from state vectors of stored waypoints. The state vectors are already included in the SEMpy software. This is achieved through iteration in the following two steps.

1. Using the Single-Shooting method, at each waypoint except the last one, the velocity is adjusted so that the subsequent segment of the trajectory ends at the next waypoint. As a result, the trajectory is continuous, but a rocket burn needs to be performed at each waypoint [8].

2. In the second step, the position and epoch of each waypoint are adjusted so that the sum of rocket burns at the waypoints results in the lowest possible need for velocity changes. These calculations yield a discontinuous trajectory [8].

This process is iterated until the discontinuity of position and velocity at each point is below a specified threshold [8].

With the Multiple-Shooting method, SEMpy generates not only the Gateway orbit in the CR3BP, but also the orbit in the ephemeris model. However, in this case, it does not generate the orbit from pre-saved waypoints but uses the CR3BP Gateway orbit as the initial guess.
The procedure is illustrated in figure 3.11. First, the CR3BP Gateway orbit is loaded (a). Then, a series of waypoints on the orbit is selected (b). Next, the step 1 described above is performed to make the orbit in the ephemeris model continuous at the waypoints (c). Subsequently, the second step, as described earlier, is applied to minimize the total velocity change requirement (d). This process is iterated (e-h) until a trajectory is calculated that has a discontinuity of state vectors at the waypoints below a tolerance threshold (h) [8]. The detailed mathematical foundations are not further discussed in the scope of this work.

In summary, the flowcharts in figures 3.8 and 3.9 differ in the red blocks as follows:
The CR3BP Gateway orbit is generated using the Multiple-Shooting method from pre-saved waypoints. The Gateway orbit in the ephemeris model is also calculated using the Multiple-Shooting method, but it uses the CR3BP Gateway orbit as the initial guess.

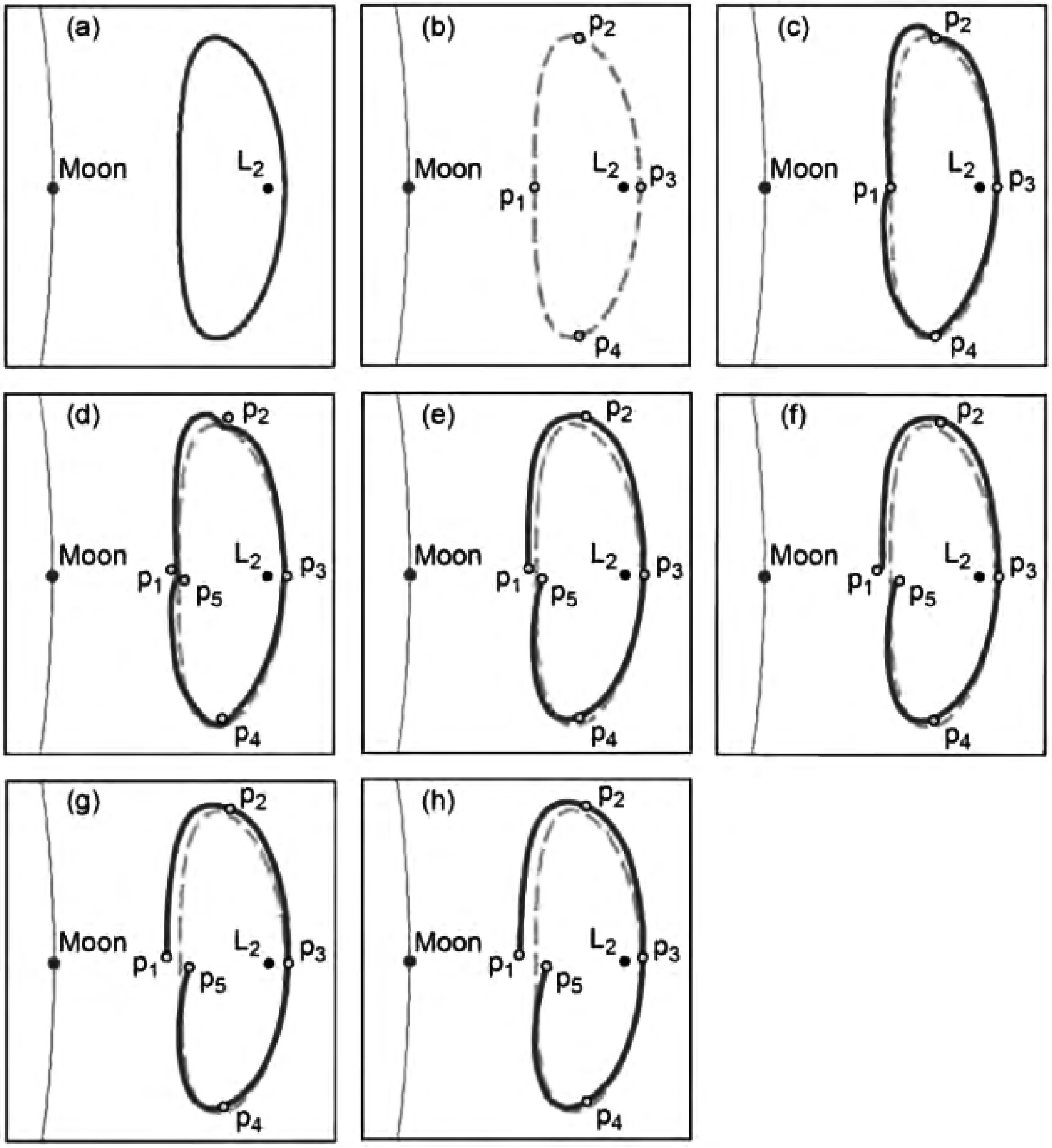

Figure 3.11: Illustration for the exemplary explanation of the individual steps of the Multiple Shooting Differential Correction method. [8]

3.4 Results of the analysis

After the introductory words and descriptions of the main foundations, this chapter now focuses on the results of the analysis of the first section of the descent. In this context, the descent from the orbit of the Gateway (see chapter 2.5, 2.6, and 3.1) to the three selected LLOs (see chapter 2.1 and 3.2) is examined.

For the analyses, calculations were performed for both one and two revolutions around the central body. However, this led to the same results, which is why only the results with an allowed number of one revolution around the central body will be presented further.
As described in chapters 1.2 and 3.3, an optimization algorithm was used in the search for the best transfer trajectories to find optimal solutions for the Lambert problems. In the context of this work, optimal means that the sum of the magnitudes of the required impulsive velocity changes at the beginning and end of the transfer is minimal. Therefore, only the transfer trajectory that requires the least amount of velocity change will be shown in the following. Naturally, there are countless other possibilities for the transfer, but they are not suitable from a orbital mechanics perspective. In addition, it should be mentioned that for the calculations it was assumed that the speed difference that has to be applied for the respective maneuver is generated by the engines in an infinitely short time. This corresponds to a burn duration of 0 s in each case.

3.4.1 Transfer from the NRHO of the Gateway to LLO 1

First, the results of the analysis of the transfer from the orbit of the Gateway to LLO 1 will be presented. As mentioned in chapter 3.2, LLO 1 is defined by the Kepler elements listed in table 3.2.

Orbit	a	e	i	Ω	ω	ν
LLO 1	1837km	0.0	$-\frac{\pi}{2}$	$\frac{\pi}{2}$	0.0	0.0

Table 3.2: Table of Kepler Elements for the selected LLO 1 used in the analysis

The LLO 1 is essentially in the same plane as the initial orbit of the Gateway, although the Gateway's orbit is only quasi-planar (see chapter 3.2).
In figure 3.12, the transfer calculated with SEMpy between the NRHO of the Gateway, computed in the CR3BP, and LLO 1 is shown.

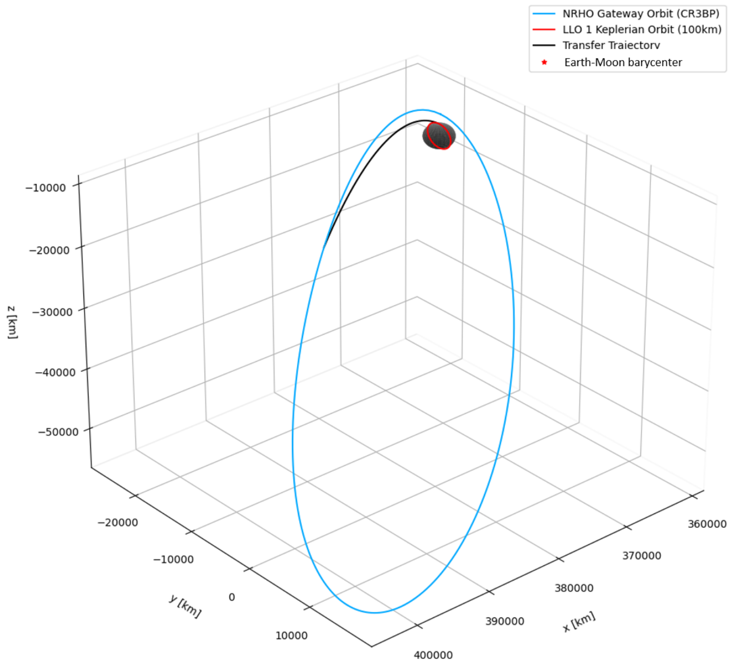

(a) Macro View

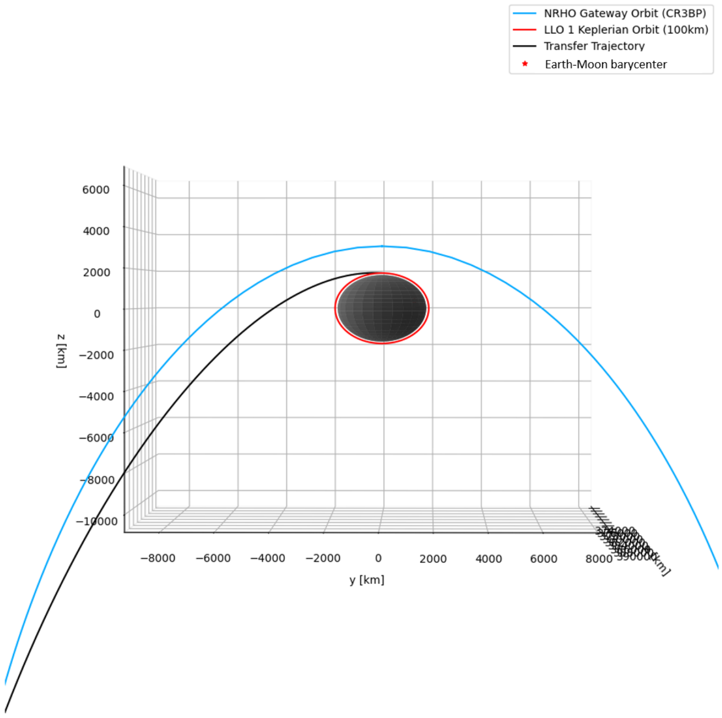

(b) Micro view

Figure 3.12: Visualization of the transfer calculated with SEMpy from the NRHO of the Gateway (CR3BP) to LLO 1

Table 3.3 lists the calculated results. Θ_1 represents the starting position of the transfer, which describes the mean anomaly on the Gateway's orbit. Θ_2 represents the end position on LLO 1. Since LLO 1 is a circular orbit, the mean anomaly and the true anomaly are equivalent in this case. Both Θ_1 and Θ_2 have a range of values from zero to one. They represent the mean anomaly divided by 2π.

Following that, the transfer time is provided, measured in days. Finally, the quantities used to evaluate the transfer, the velocity change requirements, are presented. Both the first and second maneuvers are listed separately, as well as their sum. All three quantities are given in meters per second ($\frac{m}{s}$). This format of presenting the results is also used in all subsequent tables in chapter 3.4.

Θ_1 [0, 1]	Θ_2 [0, 1]	Time of flight [days]	First dV [$\frac{m}{s}$]	Second dV [$\frac{m}{s}$]	Total dV [$\frac{m}{s}$]
0.925	0.75	0.471	50.8	688.9	739.7

Table 3.3: Table with values of the transfer from NRHO (CR3BP) to LLO 1

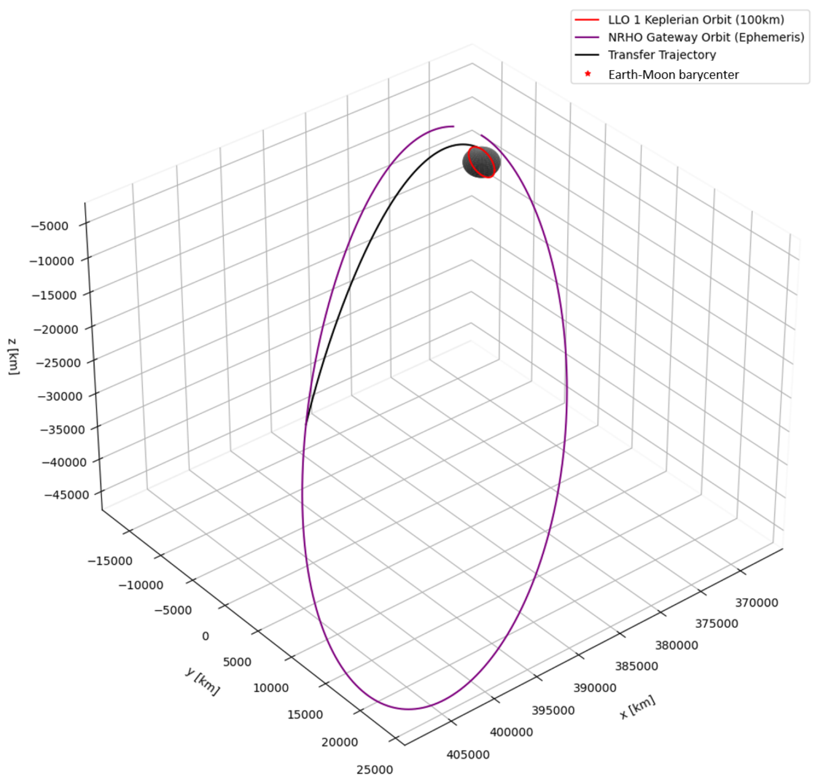

(a) Macro View

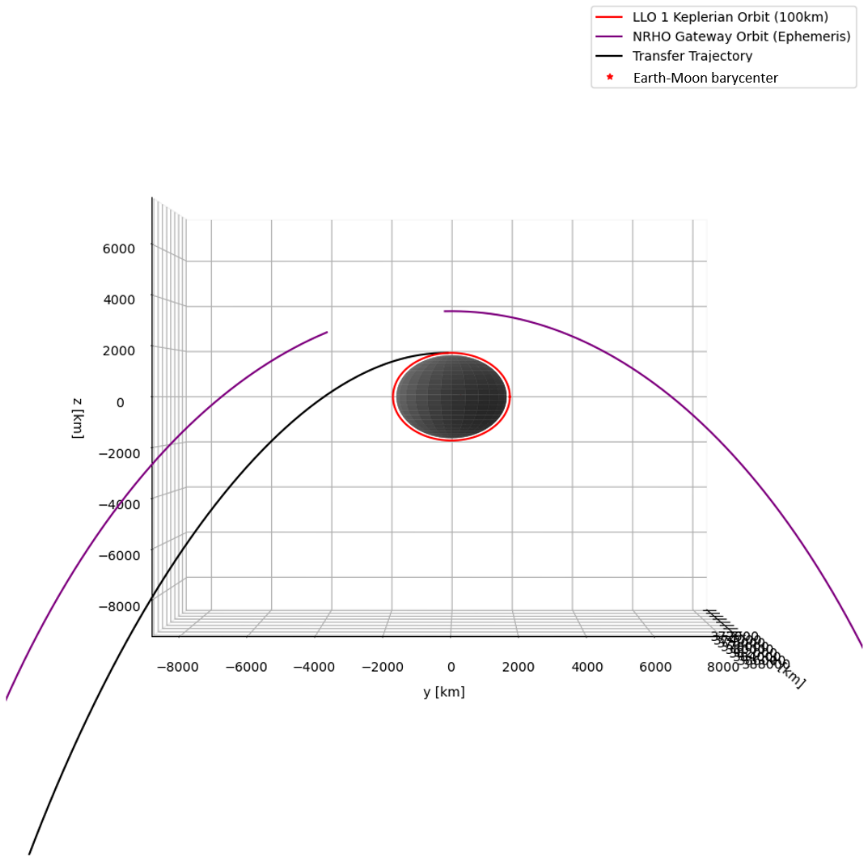

(b) Micro view

Figure 3.13: Visualization of the transfer calculated with SEMpy from the NRHO of the Gateway (ephemeris) to LLO 1

Table 3.4 presents the values of the calculated transfer from the orbit of the Gateway, computed in the ephemeris model, to LLO 1. The corresponding visualizations can be seen in figure 3.13.

Θ_1 [0, 1]	Θ_2 [0, 1]	Time of flight [days]	First dV [$\frac{m}{s}$]	Second dV [$\frac{m}{s}$]	Total dV [$\frac{m}{s}$]
0.83	0.74	1.14	47.6	725.7	773.3

Table 3.4: Table with values of the transfer from NRHO (ephemeris) to LLO 1

3.4.2 Transfer from the NRHO of the Gateway to LLO 2

The second LLO, considered as a parking orbit on the way to the Lunar surface, is the LLO 2 described in chapter 3.2. For the sake of clarity, the Kepler elements that uniquely define this orbit are once again presented in table 3.5.

Orbit	a	e	i	Ω	ω	ν
LLO 2	1837km	0.0	$-\frac{\pi}{2}$	0.0	0.0	0.0

Table 3.5: Table of Kepler Elements for the selected LLO 2 used in the analysis

The LLO 2 is rotated 90° around the z-axis compared to LLO 1. As a result of the calculation regarding a transfer from the orbit of the Gateway, computed in the CR3BP, to LLO 2, the trajectorie shown in figure 3.14 is obtained. The corresponding values of the transfer trajectory are listed in table 3.6.

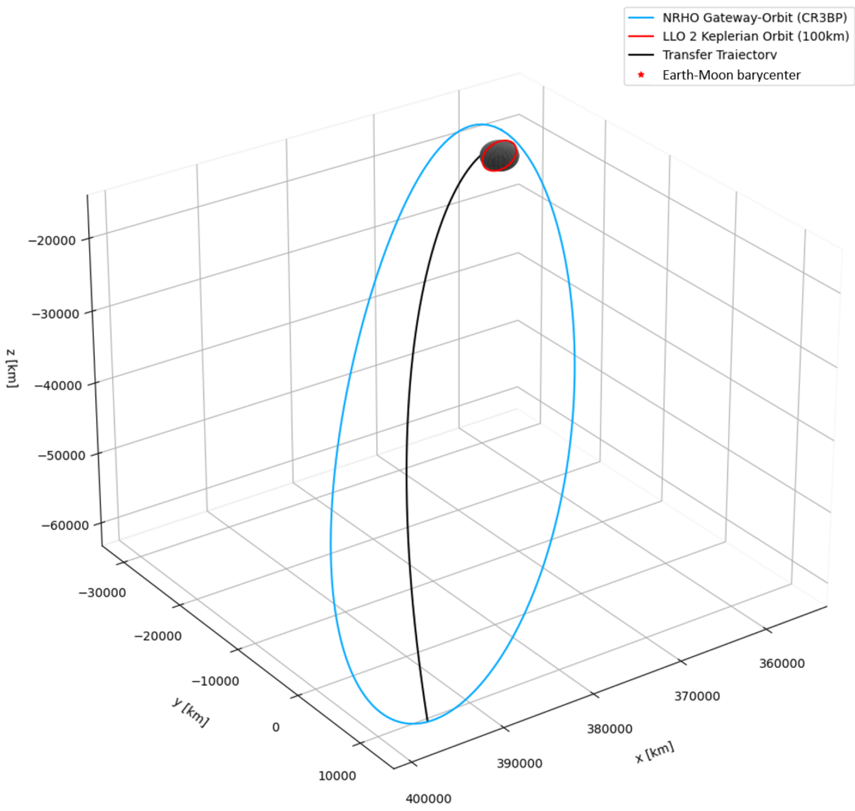

(a) Macro View

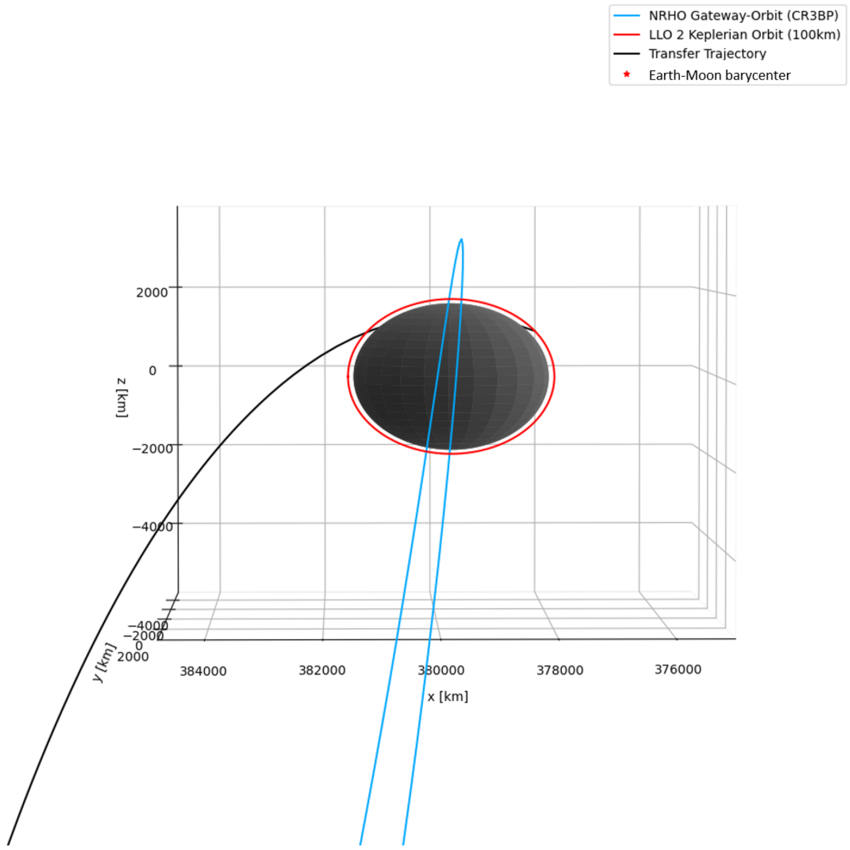

(b) Micro view

Figure 3.14: Visualization of the transfer calculated with SEMpy from the NRHO of the Gateway (CR3BP) to LLO 2

Θ_1 [0, 1]	Θ_2 [0, 1]	Time of flight [days]	First dV $[\frac{m}{s}]$	Second dV $[\frac{m}{s}]$	Total dV $[\frac{m}{s}]$
0.39	0.60	2.01	268.6	845.0	1113.6

Table 3.6: Table with values of the transfer from NRHO (CR3BP) to LLO 2

In the case of the second LLO, in addition to the calculation of the initial orbit (NRHO Gateway) in the CR3BP, a calculation using the ephemeris was also performed. The corresponding transfer trajectory is illustrated in figure 3.15. Furthermore, the associated values for the start and end positions, flight time, and required maneuvers are provided in table 3.7.

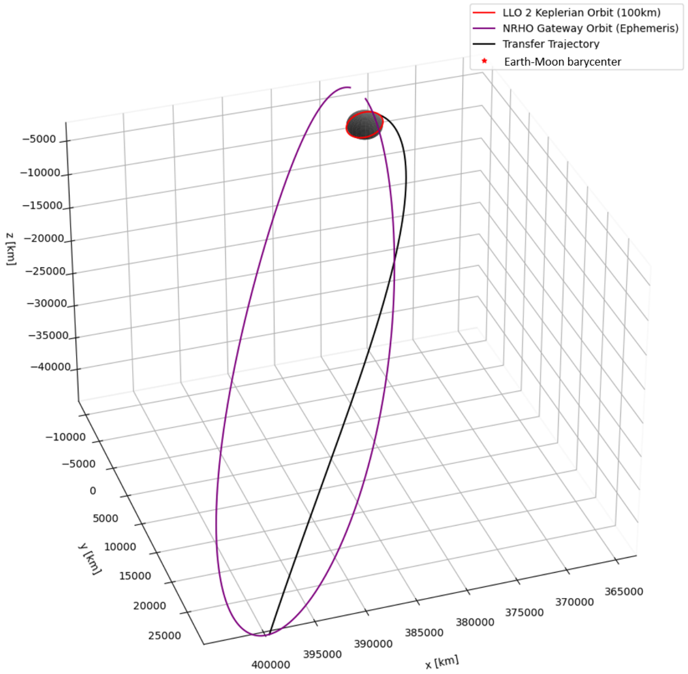

(a) Macro View

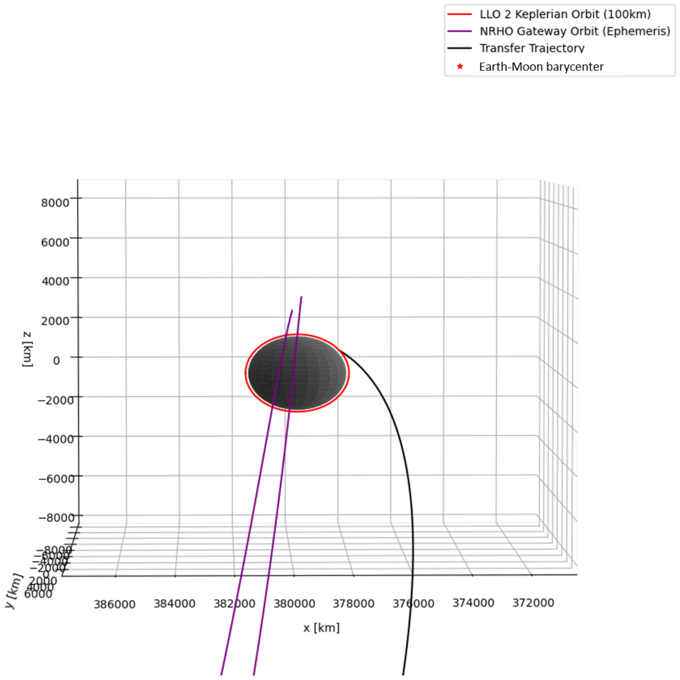

(b) Micro view

Figure 3.15: Visualization of the transfer calculated with SEMpy from the NRHO of the Gateway (ephemeris) to LLO 2

Θ_1 [0, 1]	Θ_2 [0, 1]	Time of flight [days]	First dV $[\frac{m}{s}]$	Second dV $[\frac{m}{s}]$	Total dV $[\frac{m}{s}]$
0.37	0.60	2.05	288.0	840.1	1128.1

Table 3.7: Table with values of the transfer from NRHO (ephemeris) to LLO 2

3.4.3 Transfer from the NRHO of the Gateway to LLO 3

Lastly, calculations were also performed with the equatorial LLO 3 as the target orbit. Similarly to the other two LLOs, LLO 1 and LLO 2, initial calculations were carried out using the CR3BP as the force model for the starting orbit (orbit of the Gateway). Additionally, as with the previous cases, a transfer from the orbit of the Gateway, modeled in the force model of the ephemeris, to LLO 3 was also computed. The Kepler elements defining LLO 3 are listed in table 3.8 (see chapter 3.2).

Orbit	a	e	i	Ω	ω	ν
LLO 3	1837km	0.0	0.0	0.0	0.0	0.0

Table 3.8: Table of Kepler Elements for the selected LLO 3 used in the analysis

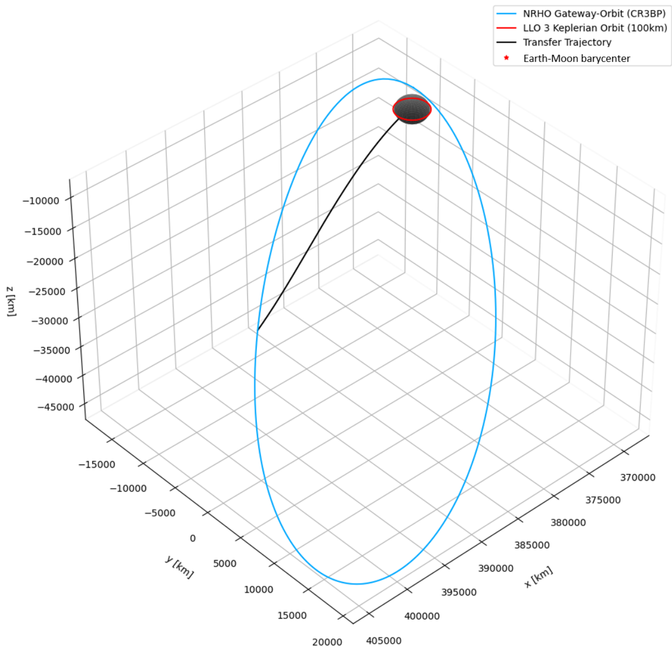

(a) Macro View

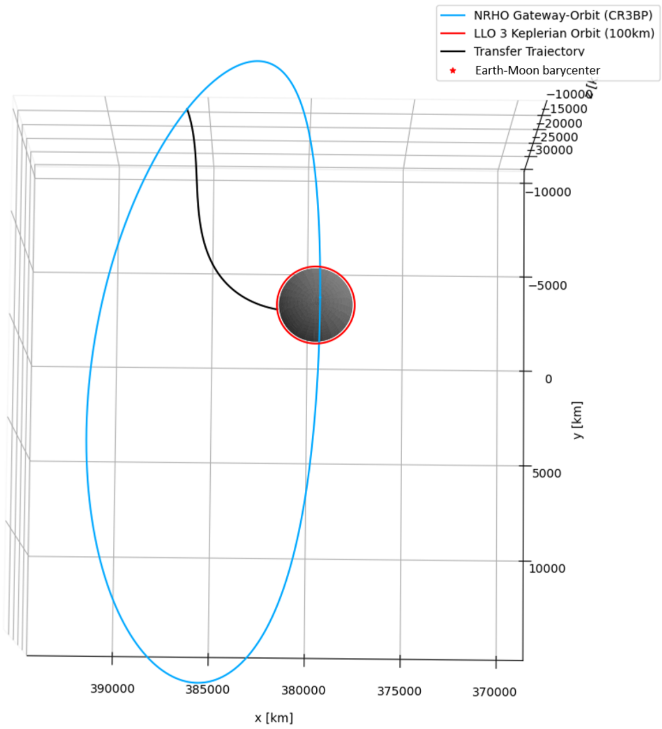

(b) Micro view

Figure 3.16: Visualization of the transfer calculated with SEMpy from the NRHO of the Gateway (CR3BP) to LLO 3

In this regard, figure 3.16 depict the computed transfer trajectory starting from the NRHO (computed in the CR3BP). The corresponding values of the transfer trajectory are listed in table 3.9.

Θ_1 [0, 1]	Θ_2 [0, 1]	Time of flight [days]	First dV $[\frac{m}{s}]$	Second dV $[\frac{m}{s}]$	Total dV $[\frac{m}{s}]$
0.83	0.02	1.12	146.6	2407.0	2553.6

Table 3.9: Table with values of the transfer from NRHO (CR3BP) to LLO 3

Finally, figure 3.17 depict the computed trajectory of the transfer from the orbit of the Gateway (ephemeris model) to LLO 3. The corresponding values of the transfer are listed in table 3.10 below.

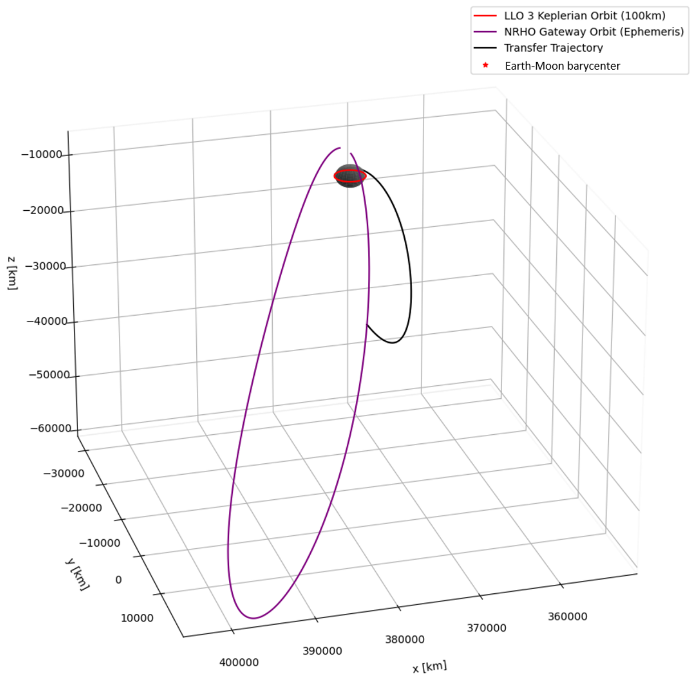

(a) Macro View

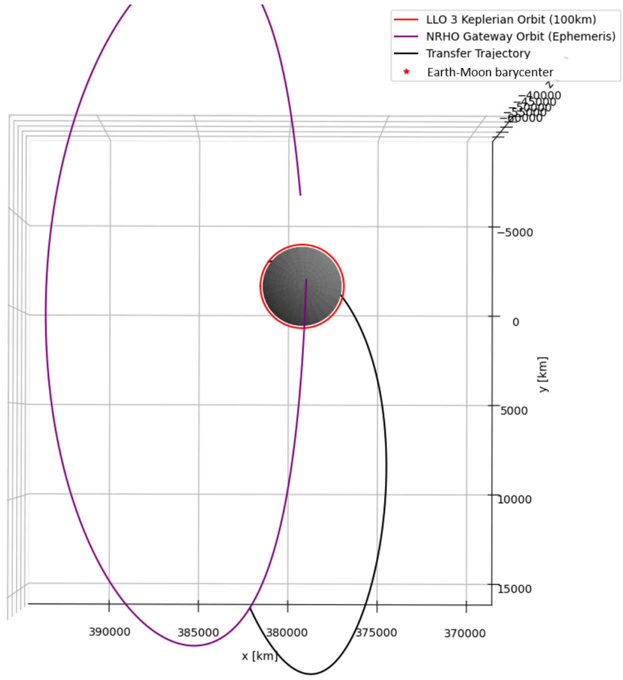

(b) Micro view

Figure 3.17: Visualization of the transfer calculated with SEMpy from the NRHO of the Gateway (ephemeris) to LLO 3

Θ_1 [0, 1]	Θ_2 [0, 1]	Time of flight [days]	First dV [$\frac{m}{s}$]	Second dV [$\frac{m}{s}$]	Total dV [$\frac{m}{s}$]
0.05	0.9	1.14	458.0	1909.4	2367.4

Table 3.10: Table with values of the transfer from NRHO (ephemeris) to LLO 3

3.4.4 Evaluation of the results

After presenting the obtained results of the calculations for the descent trajectory from the orbit of the Gateway to the three parking orbits, LLO 1, LLO 2, and LLO 3, in chapters 3.4.1, 3.4.2, and 3.4.3, respectively, it is now time to evaluate and analyze these results. A summary of the values for each transfer trajectory is provided in table 3.11. To enhance clarity, the sums of the velocity changes are highlighted in light blue when the orbit of the Gateway was computed using the CR3BP, and in purple when the orbit of the Gateway was computed using the ephemerides.

Target Orbit	Force model of NRHO	Θ_1 [0, 1]	Θ_2 [0, 1]	Time of flight [days]	First dV [$\frac{m}{s}$]	Second dV [$\frac{m}{s}$]	Total dV [$\frac{m}{s}$]
LLO 1	CR3BP	0.925	0.75	0.471	50.8	688.9	739.7
LLO 1	ephe-merides	0.83	0.74	1.14	47.6	725.7	773.3
LLO 2	CR3BP	0.39	0.60	2.01	268.6	845.0	1113.6
LLO 2	ephe-merides	0.37	0.60	2.05	288.0	840.1	1128.1
LLO 3	CR3BP	0.83	0.02	1.12	146.6	2407.0	2553.6
LLO 3	ephe-merides	0.05	0.9	1.14	458.0	1909.4	2367.4

Table 3.11: Table of values for all calculated transfers from the NRHO to LLO 1, LLO 2, and LLO 3

In general, the results show that a transfer to LLO 1 is the most favorable in terms of velocity change requirement. Here, the values obtained are 739.7 $\frac{\mathrm{m}}{\mathrm{s}}$ (NRHO - CR3BP) and 773.3 $\frac{\mathrm{m}}{\mathrm{s}}$ (NRHO - Ephemeriden). These values are not too far from the value of 707 $\frac{\mathrm{m}}{\mathrm{s}}$ mentioned by Whitley et al. [34] in their work for a transfer from the Gateway orbit to a polar LLO.

Furthermore, it can be observed that a transfer to LLO 2 requires a velocity change of approximately 375 $\frac{\mathrm{m}}{\mathrm{s}}$ (CR3BP) or 355 $\frac{\mathrm{m}}{\mathrm{s}}$ (Ephemeriden) more than the transfer to LLO 1. This pattern continues for the computed transfers to LLO 3. In both cases (CR3BP and Ephemeriden), a velocity change requirement is needed that is more than twice as large as that for a transfer to LLO 2.
The explanation for these results lies in the orientation of the LLO 2 and LLO 3 orbits in space. They are rotated 90 degrees relative to the coarse plane of NRHO. The velocity change required to perform a rotation of the orbital plane through a maneuver is given by Whitley et al. [34] using equation 3.1. Here, Δv represents the velocity change required for a change in the orbital plane, v is the magnitude of the spacecraft velocity at the point where the maneuver is performed, and Δi represents the angle by which the orbital plane is to be rotated.

$$\Delta v = 2 \cdot v \cdot sin\left(\frac{\Delta i}{2}\right) \tag{3.1}$$

Using equation 3.1, it follows that the velocity change requirement increases with the angle for a change in the orbital plane. The maximum value is reached for a plane change of 90 degrees. A plane change of 91 degrees would be more challenging according to the equation, but such a rotation of the orbital plane is equivalent to a rotation of 89 degrees in the opposite direction. Therefore, a 90-degree rotation of the orbital plane during a transfer results in the maximum velocity change requirement. Consequently, transfers to LLO2 and LLO3 each represent the worst possible case and have extremely large velocity change requirements.

Nonetheless, it can also be deduced from the equation that the required velocity change increases linearly with the velocity of the spacecraft, as v appears as a linear factor in the equation. Therefore, it is more sensible to perform the plane change at lower velocities. This is the case when the spacecraft is near the apolune, where the minimum velocity on the orbit is present. Hence, if a plane change needs to be performed, it is advisable to initiate the transfer near or at the apolune.
In figure 3.14 of the transfer from NRHO to LLO 2, it can be seen that this is approximately the case there. However, the transfers to LLO 3, shown in figures 3.16 and 3.17, start further away from the apolune of NRHO. This ultimately results in a higher spacecraft velocity during the maneuver, which in turn contributes to the required velocity changes of the transfer to LLO 3 in table 3.11.
Therefore, it can be said that the results are quite robust, and the significant changes in velocity change requirements can be explained by the performed plane changes. It is also noteworthy that it is advisable to initiate a descent to the Lunar surface from a polar LLO. This is because an orbit is required to fly over a specific point on the Lunar surface, and this can be achieved for all points on the Lunar surface as the ground tracks of all possible polar LLOs cover the entire Lunar surface.

However, the computed transfers must also be critically examined. Two out of the six calculated transfer trajectories pass through the Lunar surface. The reason for this cannot be attributed to the CR3BP or the Ephemeriden themselves, as this error occurs in both calculation methods. These instances are marked by orange circles in figures 3.18 and 3.19.
To explain this behavior, we need to consider the assumptions that were made. Since the Moon is assumed as a point mass and no further constraints regarding potential obstacles such as the Moon itself are taken into account during the trajectory calculation, the gravitational field of the Moon is considered in the calculation, but the Moon as a physical body is not. Therefore, for a real application of these two trajectories, an adjustment would need to be made to avoid collision with the Lunar surface.

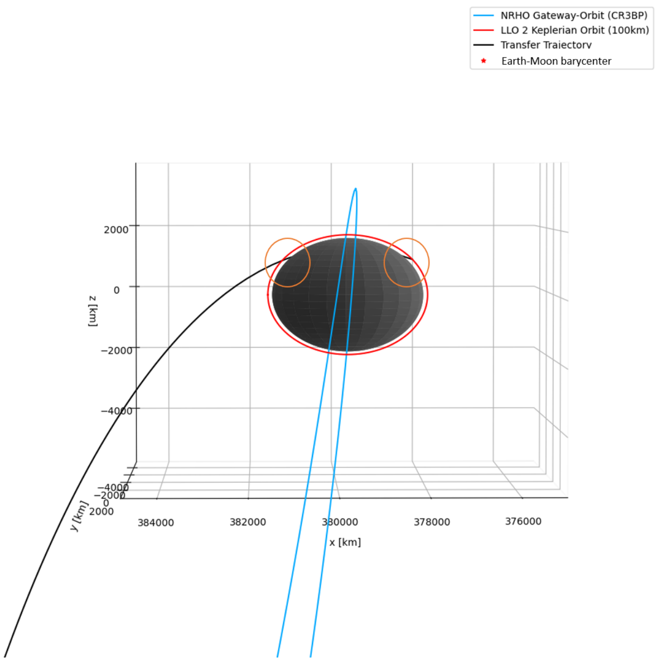

Figure 3.18: Visualization of the transfer calculated using SEMpy from the NRHO of the Gateway (CR3BP) to LLO 2 with markings indicating the intersection points with the Lunar surface

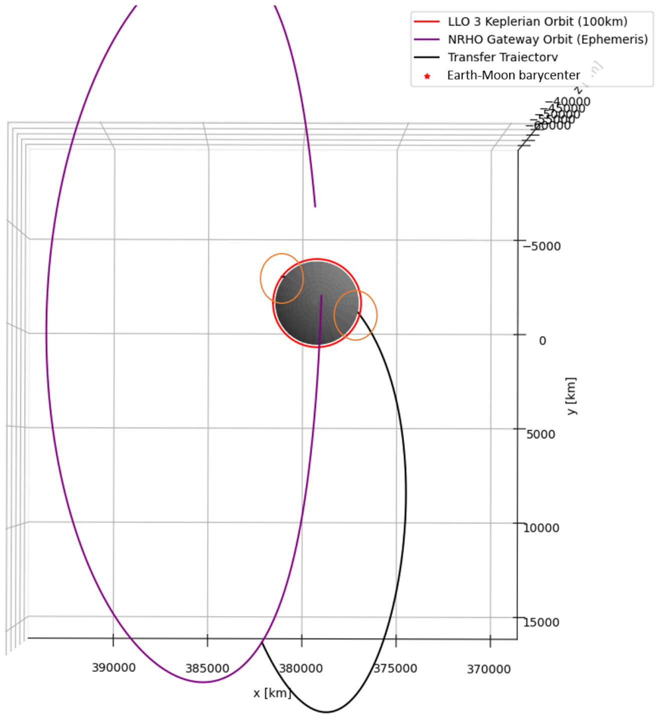

Figure 3.19: Visualization of the transfer calculated using SEMpy from the NRHO of the Gateway (ephemerides) to LLO 3 with markings indicating the intersection points with the Lunar surface

In summary, regarding the orbital mechanics considerations of this work, it can be stated that the initially defined objective (see chapter 1.1) of analyzing descent trajectories from the Gateway's orbit to different LLOs has been achieved.
Within the available resources, transfer trajectories from the Gateway's orbit in the CR3BP as well as in the Ephemeriden model to the specified LLOs were calculated. From the results of the calculations, the trajectory with the lowest velocity change requirement for each type of transfer, and whose flight time is also within an acceptable range, was presented in the context of the work.

3.5 Descent from the LLOs to the Lunar surface

After examining the descent from the Gateway's orbit to the LLOs in the previous chapters, this chapter will now focus on the further descent from the LLOs to the Lunar surface. In the following, as described at the beginning in chapters 1.1 and 1.2, only a theoretical consideration will be conducted.
In general, it can be said that the LLO chosen as an intermediate station for the descent to a specific landing point should be selected in a way that the LLO flies over the landing point. This eliminates the need for additional plane change maneuvers during the descent to the surface, reducing fuel consumption and velocity change requirements. Once the spacecraft has arrived on the respective LLO through a transfer, as presented in chapters 3.4.1 to 3.4.3, the subsequent descent to the Lunar surface follows the same procedure. This approach is independent of the choice of LLO.

In general, it can be said that a descent to the Lunar surface requires a reduction of the descent rate to a value at which the landing module is not damaged or destroyed upon impact. This occurs at a descent rate of approximately $2\,\frac{\mathrm{m}}{\mathrm{s}}$ or less. To achieve this, the firing of the engines is the only viable option in case of the Moon, as parachutes cannot be used due to the absence of an atmosphere. To accomplish this, the descent can be divided into three steps [9]. These steps are as follows in chronological order:

1. Deorbit Burn
2. Coast Phase
3. Powered Descent

These steps are exemplified in figure 3.20. Initially, the spacecraft is at an altitude of 100 km in a circular LLO, and without further maneuvers, it would continue to orbit the Moon at this altitude. This altitude corresponds to the height of the LLOs chosen as parking orbits in chapters 3.4.1 to 3.4.3. To initiate the descent, the first step in the sequence is the deorbit burn. The engine is ignited to achieve a velocity change of approximately $18.6\,\frac{\mathrm{m}}{\mathrm{s}}$ (1.). This brings the spacecraft onto a Hohmann transfer ellipse closer to the Lunar surface. The flight along the transfer ellipse is carried out without further maneuvers and is referred to as the coast phase (2.) [9].

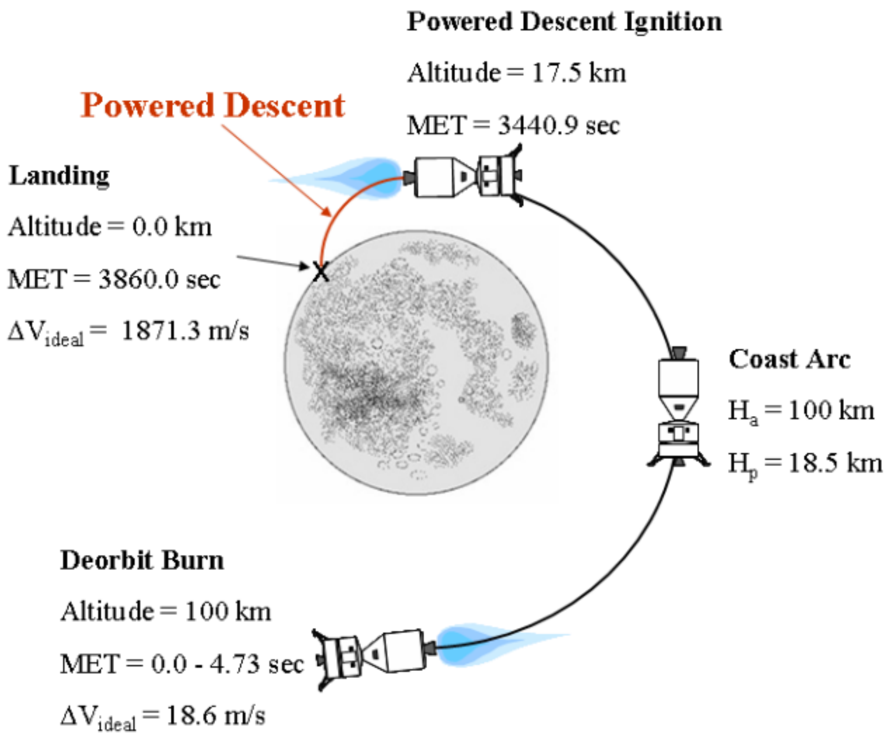

Figure 3.20: Exemplary illustration of the descent and landing process from a 100 km circular orbit to the Lunar surface [9]

On the opposite side of the Moon, the closest approach to the Lunar surface on the transfer ellipse is reached at an altitude of approximately 17.5 km. At this point, the final descent phase begins with the ignition of the engines (Powered Descent Ignition) (3.). This last part of the descent is the most complex and can be further divided into three phases, which are named as follows [9]:

3.1 Braking Phase

3.2 Approach Phase

3.3 Terminal Descent Phase

The overall fuel consumption during this third part of the descent, with a rough velocity change requirement of 1871.3 $\frac{\mathrm{m}}{\mathrm{s}}$ (see figure 3.20), is the highest. This is because the spacecraft needs to decelerate from orbital velocity to 0 $\frac{\mathrm{m}}{\mathrm{s}}$ during this phase. Additionally, continuous maneuvers are performed during the powered descent to control the spacecraft's orientation [9].

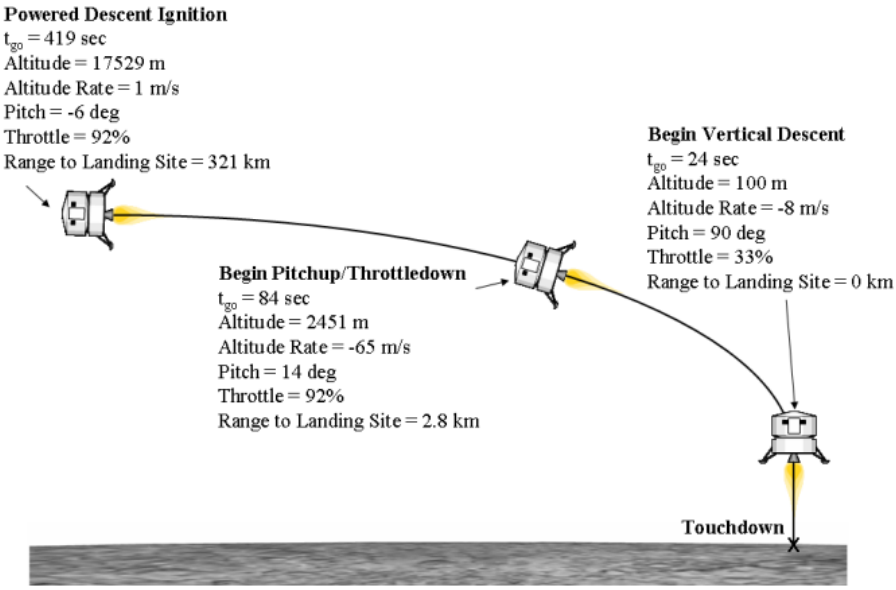

Figure 3.21: Exemplary Representation of Powered Descent as the Final Phase of Descent to the Lunar Surface [9]

The first step of the powered descent, as shown in figure 3.21, is the ignition of the engines (3.). This initiates the braking phase, which is the longest phase of the final step of the descent (3.1). It is designed for the engine to operate at roughly 92% of its maximum thrust, to maintain a reserve of thrust for emergency maneuvers. The braking phase is responsible for reducing the majority of the spacecraft's velocity [9].

Following that, in step 3.2, is the approach or pitch-up phase. It begins approximately 84 seconds before landing and is responsible for orienting the spacecraft vertically towards the surface to enable a vertical landing. During this phase, the braking engines, which are still operating at 92% thrust from the braking phase (3.1), are gradually throttled down. Additionally, the attitude control thrusters along the pitch axis (lateral axis) are fired evenly to initiate a controlled rotation of the spacecraft into the vertical position [9].

As a result of the preceding maneuvers, the spacecraft is positioned approximately 100 meters vertically above the landing point. From there, it descends vertically with an engine thrust level of approximately 33% of maximum thrust (1.2 Moon G's) before finally touching down at the desired landing point [9]. The percentage values of thrust are provided for better clarity and are based on the analysis by Jerry Condon (NASA) regarding an initial Lunar outpost [35].

A similar descent sequence was used in the NASA Apollo program. A visual representation of the third section (Powered Descent) is shown in figure 3.22. It can be observed that the Deorbit Burn (1.) is designed to bring the spacecraft to a point 15km above the surface at the end of the transfer ellipse (Coasting Phase - 2.). From there, the Powered Descent Ignition initiates the Powered Descent Phase shown in figure 3.22 (3.). All further steps correspond accordingly to the descent process described above [9].

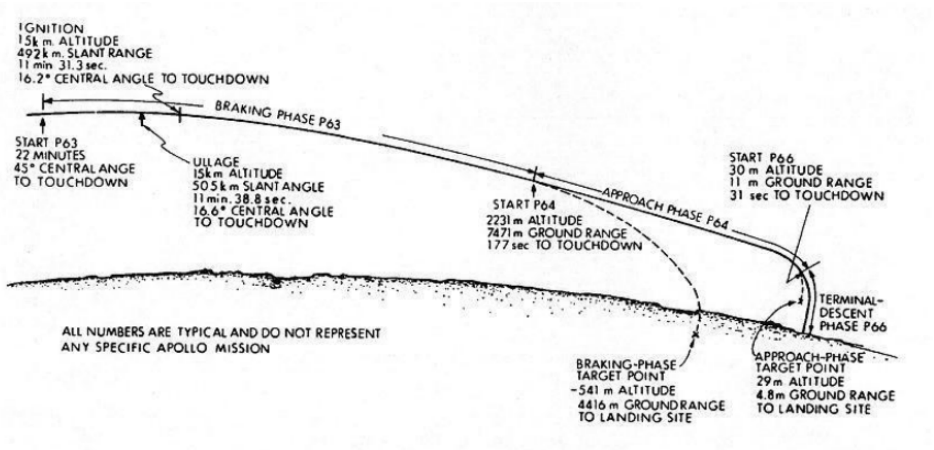

Figure 3.22: Visualization of the Powered Descent of the NASA Apollo Program [9]

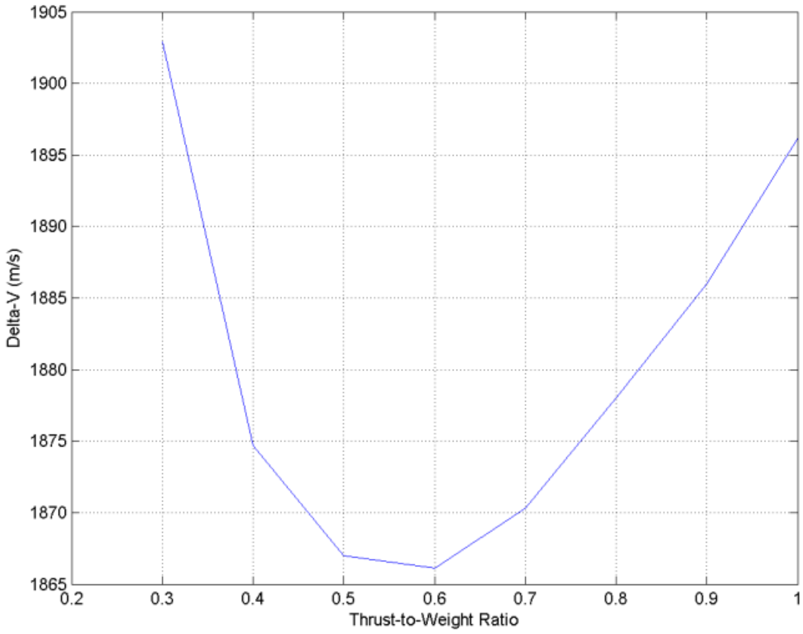

Figure 3.23: Visualization of the Total Velocity Change Required for Descent from a 100km Circular Lunar Orbit to the Surface against the Thrust-to-Weight Ratio [9]

The further analysis by Sostaric et al. [9] revealed that the total velocity change requirement depends on the thrust-to-weight ratio. This is shown in figure 3.23. The velocity change requirement ranges from 1866 $\frac{\mathrm{m}}{\mathrm{s}}$ to 1903 $\frac{\mathrm{m}}{\mathrm{s}}$ as a function of the thrust-to-weight ratio. This applies to a descent from a 100 km circular Lunar orbit, with a Powered Descent Ignition at an altitude of 18.5 km and a touchdown velocity of 2 $\frac{\mathrm{m}}{\mathrm{s}}$. Including a gravity turn for the descent, the analysis yielded an even lower value of 1716.5 $\frac{\mathrm{m}}{\mathrm{s}}$. However, it must be noted that this procedure has been carried out before, but is not yet used as a common procedure [9].

In conclusion, it can be stated that the velocity change requirement for descent from a 100 km circular Lunar orbit, considering safety margins for potential emergencies, is approximately 2000 $\frac{\mathrm{m}}{\mathrm{s}}$. This aligns with the velocity change requirement of 2055 $\frac{\mathrm{m}}{\mathrm{s}}$ planned for the Powered Descent phase of the Apollo mission [9]. Furthermore, Whitley et al. [34] mention a value of 2100 $\frac{\mathrm{m}}{\mathrm{s}}$ for descent and 1900 $\frac{\mathrm{m}}{\mathrm{s}}$ for ascent to/from a 100km circular Lunar orbit. Therefore, a value of 4000 $\frac{\mathrm{m}}{\mathrm{s}}$ is chosen as a comparison value for the case analysis in the following chapters 3.6.1 and 3.6.2.

3.6 Case studies

To put the results of chapter 3.4 into a real context, the calculated transfer trajectories will now be evaluated for their feasibility based on two case studies. Firstly, the Orion capsule of NASA and the propulsion system of its associated European Service Module (ESM) by ESA will be considered. Secondly, the propulsion system of SpaceX's Starship, developed by the private company SpaceX, will be used for the calculations.

As described at the beginning (see chapter 1), these two systems were chosen because they are intended for operation by NASA for the Gateway. The technical specifications of the two systems used in the following sections are not only derived from official sources but also from non-official sources, which means they may not be entirely accurate. Nevertheless, they are sufficient for an initial estimation within the scope of this work.

3.6.1 Orion Capsule and European Service Module

One of the spacecraft that is considered for actual Lunar missions is the NASA's Orion capsule. It is a crucial component of the Artemis program and is designed to transport astronauts from Earth's orbit to the Moon and back to Earth.
Another essential component in connection with the Orion capsule is the ESM. This module is built by Airbus on behalf of ESA and is handed over to NASA upon completion. The ESM is located beneath the Orion capsule and provides critical functions such as propulsion (attitude and orbit control), thermal control, and electrical power [10]. Figure 3.24 shows a photo of the Orion capsule with the attached ESM of the Artemis I mission.

Since this example aims to contextualize the acquired insights, the propulsion system of the ESM is of particular interest for further analysis. The main engine of the ESM is a previously used engine from the Orbital Maneuvering System of NASA's Space Shuttles [36].

Figure 3.24: Photo of the Orion capsule and the attached ESM of the Artemis I mission at the Neil Armstrong Operations and Checkout Building at NASA's Kennedy Space Center in Florida [10]

In order to perform the necessary calculations, we will first consider the Tsiolkovsky equation, also known as the rocket equation, which is represented by equation 3.2 [1].

$$\Delta v = g_0 \cdot I_{sp} \cdot ln\left(\frac{m_i}{m_f}\right) \tag{3.2}$$

Δv represents the change in velocity that a spacecraft undergoes by burning propellant with a mass of $m_{pr} = m_i - m_f$ and expelling the combustion gases with a velocity of $c_e = g_0 \cdot I_{sp}$. Here, g_0 denotes the acceleration due to Earth's gravity. For the following calculations, a value of $g_0 = 9.81\,\frac{\mathrm{m}}{\mathrm{s}^2}$ was used. I_{sp} describes the specific impulse of the engine. Since all calculated transfers take place in a vacuum, the specific impulse for a vacuum is used. For the ESM engine, this value is $I_{sp} = 316\,\mathrm{s}$ [37]. Rearranging equation 3.2 yields equation 3.3.

$$\frac{m_i}{m_f} = e^{\frac{\Delta v}{I_{sp} \cdot g_0}} \tag{3.3}$$

In addition, the values for the velocity change requirement Δv listed in table 3.12 from chapter 3.4 are used. By calculating with equation 3.3, the ratios of total mass before and after the maneuver $\frac{m_i}{m_f}$, as shown in table 3.12, are obtained.

Start orbit	Target orbit	Δv $\left[\frac{\mathrm{m}}{\mathrm{s}}\right]$	$\frac{m_i}{m_f}$	m_{pr} [t]
NRHO (ephemerides)	LLO 1	773.3	1.283	5.4
NRHO (ephemerides)	LLO 2	1128.1	1.439	7.5
NRHO (ephemerides)	LLO 3	2367.4	2.146	13.1

Table 3.12: Table of velocity change requirements depending on the starting and target orbits, the corresponding required initial-to-final mass ratio, and the corresponding propellant requirements

For the Orion capsule, an initial weight m_i of 24 584.7 kg (9 298.6 kg - Crew Module, 15 286.1 kg - ESM) is assumed in this analysis [10]. Thus, with a capsule initially filled with full tanks, the corresponding propellant requirement m_{pr} for each transfer listed in table 3.12 can be derived.

Additionally, assuming a total available propellant mass of 9 metric tons [36], the mass of the Orion capsule when all the propellant is consumed would be 15 584.7 kg, resulting in a initial-to-final mass ratio of $\frac{m_i}{m_f} = 1.61$. If the value of each transfer is below 1.61, the transfer is possible with a fully fueled Orion capsule. If it is above 1.61, more propellant is needed for the transfer than available in the capsule's tanks, making the transfer impossible without refueling. This is also evident from the values of the required propellant mass.

Consequently, the analysis in this work shows that the transfers calculated from NRHO to LLO 1 and LLO 2 in chapter 3.4 are feasible with an Orion capsule. However, the capsule should be refueled upon arrival from Earth at the Gateway to safely descend to one of the LLOs, as the flight from Earth to the Gateway also requires propellant. Additionally, the capsule must be refueled again after arrival in the LLO for the return journey, as the return flight to the Gateway would otherwise be impossible. A flight to LLO 3 with the calculated transfer in chapter 3.4 is not possible with an Orion capsule, as the propellant requirement of 13.1 metric tons exceeds the available propellant of 9 metric tons.

3.6.2 SpaceX Starship

The second spacecraft intended to fly to the Moon within the coming years is SpaceX's Starship. It serves as the second stage of the Starship system, which consists of the second stage (Starship) and the Super Heavy booster as its first stage.
The Starship itself has a fuel capacity of 1,200 metric tons and a payload capacity of 100 to 150 metric tons [12]. Figure 3.25 displays a photo of the Starship mounted on the Super Heavy booster for a test flight.

Figure 3.25: Photo of SpaceX's Starship mounted on the Super Heavy booster for a test flight. [11]

The Starship is powered by a total of six Raptor engines (see figure 3.26). Among them, three engines are designed for operation in the atmosphere, while the remaining three engines are optimized for vacuum operation. Therefore, the fuel requirements are calculated using the values specific to the vacuum variant, resulting in a specific impulse of $I_{sp} = 363\,\mathrm{s}$ in a vacuum [38]. Furthermore, the total weight of the Starship is 1 300 metric tons, with a fuel mass component of 1 200 metric tons [39].
The calculations in this case study are carried out in the same manner as in the previous chapter 3.6.1, using equation 3.3.

Figure 3.26: Graphic of a Raptor engine of SpaceX's Starship [12]

The results of the calculations are listed in table 3.13. When using a total mass m_i of 1 300 metric tons and a propellant mass m_{pr} of 1 200 metric tons, the ratio of initial to final mass $\frac{m_i}{m_f}$ after burning all the propellant is 13.

Start orbit	Target orbit	Δv $\left[\frac{\text{m}}{\text{s}}\right]$	$\frac{m_i}{m_f}$	m_{pr} [t]
NRHO (ephemerides)	LLO 1	773.3	1.242	253.1
NRHO (ephemerides)	LLO 2	1128.1	1.373	353.2
NRHO (ephemerides)	LLO 3	2367.4	1.944	631.3

Table 3.13: Table of speed change requirements depending on the starting and target orbits, the respective necessary ratio of initial-to-final mass, and the corresponding fuel requirements

Accordingly, all the calculated transfers from the Gateway to the LLOs are possible with a fully fueled Starship, as shown in table 3.13. For the transfers to LLO 1 and 2, even a return trip with the same velocity change requirements would be easily achievable.
Since the Starship has the capability to land and take off again, which the Orion capsule does not have, it is also useful to calculate the propellant consumption for a subsequent descent to the Lunar surface. For this purpose, we assume the first part of the descent, the transfer from NRHO to LLO 1. This results in a starting mass of $m_i = 1300\,\mathrm{t} - 253.1\,\mathrm{t} = 1046.9\,\mathrm{t}$. Using equation 3.3 and a velocity change requirement of $4000\,\frac{\mathrm{m}}{\mathrm{s}}$ (see chapter 3.5), the propellant requirement is calculated to be $m_{pr} = 706.5\,\mathrm{t}$. This leads to a total propellant requirement for the descent to LLO 1, the descent to the Lunar surface, and the ascent back to LLO 1 of $m_{pr,ges} = 959.6\,\mathrm{t}$. Accordingly, there is still some propellant left for the ascent to NRHO of $m_{pr,re} = 1200\,\mathrm{t} - 959.6\,\mathrm{t} = 240.4\,\mathrm{t}$. However, since safety reserves are necessary anyway, refueling on the Lunar surface is required and can be easily accomplished with the planned infrastructure there.

3.6.3 Results of the case studies

Overall, from the two case studies in chapters 3.6.1 and 3.6.2, it can be concluded that both systems are capable of flying at least a part of the calculated trajectories from NRHO to the LLOs. The Orion capsule can perform the transfers from NRHO to LLOs 1 and 2. With the Starship's propellant capacity, flights to all three LLOs are possible. In the case of LLOs 1 and 2, a return trip is also easily achievable with the Starship. Furthermore, the Starship is capable of handling the transfer to LLO 1, the descent to the Lunar surface, and the ascent with its propellant capacities.
However, it is essential to consider the need for refueling in orbit or on the Lunar surface. Both systems first complete the journey from Earth's orbit to the Gateway's Lunar orbit, requiring additional propellant. Therefore, both systems should be refueled upon their arrival at the Gateway. This requires on-site infrastructure and the availability of propellant. This aspect must be taken into account in the planning of Gateway operations and manned flights to the Lunar surface.
In case of a Lunar landing, the possibility of refueling on the Moon should also be considered. This can be accomplished either through a Lunar base or a tanker that lands on the Moon as well.

Chapter 4

Operational analysis of the descent trajectory

In addition to the orbital mechanics aspects discussed in chapter 3, this work also considers operational aspects of the descent trajectories from the Gateway's orbit to the LLOs. This means that in the following sections, the flight times, communication possibilities, and eclipses during the transfer trajectories presented in chapters 3.4.1 to 3.4.3 will be analyzed and evaluated.
These three areas are essential aspects of manned spaceflight, as crew safety is paramount. Therefore, the analyses that follow are specific to flights with manned spacecraft. The trajectories presented in chapters 3.4.1 to 3.4.3 are also already tailored to this application. For cargo flights, trajectories could be designed with much longer flight times, resulting in significantly lower velocity change requirements and fuel consumption.

4.1 Time of flight

The flight duration of a transfer is one of the most relevant factors in the context of manned spaceflight, as it has a significant impact on the design of the spacecraft. The longer the flight, the more equipment a spacecraft requires. The crew's oxygen, water, and food supply must be ensured. Adequate reserves must also be allocated to mitigate any deviations from the mission plan and to ensure the crew's safety. Additionally, for longer transfers, there needs to be enough space within the spacecraft for the crew to have rest areas and move around. Lastly, provisions for waste management, including toilet facilities, must be considered.
These various factors quickly add up when planning longer missions. They inevitably lead to increased spacecraft mass, which in turn necessitates higher fuel consumption. Furthermore, a larger physical volume and more complex construction are required, as the difficulty of building a pressurized capsule increases with its size.

For these reasons, the flight duration was limited to 3 days in the analyses presented here. This value represented the upper limit of possible flight durations in the optimization of transfer trajectories discussed earlier (see chapters 3.3 and 3.4.1 to 3.4.3). A transfer time of 0 was used as the lower limit, allowing the optimizer to consider all values between 0 and 3 days to find the most fuel-efficient transfer. A starting value of half a day was used for the optimizations performed, which resulted in the flight durations listed in table 4.1 (see also table 3.11).

Target orbit	Force model NRHO	Time of flight [days]
LLO 1	CR3BP	0.471
LLO 1	ephemerides	1.14
LLO 2	CR3BP	2.01
LLO 2	ephemerides	2.05
LLO 3	CR3BP	1.12
LLO 3	ephemerides	1.14

Table 4.1: Table of Time of flights for all calculated Transfers from the NRHO to LLO 1, 2, and 3

From table 4.1, it can be observed that none of the calculated transfers exceed 2 days in duration. However, even a 2-day transfer should not be underestimated and requires careful mission planning. Therefore, it is recommended to prefer transfers that take one day (transfers to LLOs 1 and 3), as this reduces the complexity of the descent to the Lunar surface.

4.2 Communication links

After evaluating the flight durations, it is important to examine the stability of the communication link during the transfer. In addition to life-support measures on board the spacecraft, a reliable communication link with the mission control center is crucial. The communication link is used to transmit telemetry data from the spacecraft to the ground-based mission centers. This includes all relevant technical parameters that must fall within specific ranges to ensure the proper functioning of all spacecraft systems. This allows the respective expert teams for subsystems such as the Attitude and Orbit Control System (AOCS) or the Thermal Control System (TCS) to identify and address any issues that may arise during the mission.
Furthermore, in the event of a mission abort or for other reasons, it may be necessary to modify the spacecraft's current trajectory. In such cases, a communication link is essential for uploading the new mission profile and the required maneuvers (sequence of engine burns) into the navigation computer.

4.2.1 Network of used ground stations

To establish a communication link between a spacecraft and a control center, a ground station is required. The ground station receives signals from the spacecraft using large antennas, processes them, and makes them available for use by the control center. A ground station is also capable of sending signals to the spacecraft, such as radio communications to the crew or commands to the onboard computer.
In the context of this work, a mission near the Moon is considered. As a result, the distance between the spacecraft and the ground station is very large (approximately 385 000 km). This means that the signals transmitted by the spacecraft are significantly attenuated due to the long distance (known as *Free Space Path Loss*). Additionally, other disturbances such as atmospheric effects can further affect the signal. Furthermore, it is not possible to amplify the spacecraft's transmitted signal, as it would require a very high electrical power that cannot be generated on board a spacecraft.
Therefore, the use of very large antennas (with diameters of $\geq$ 30m) is necessary to receive enough power from the transmitted signal, despite the disturbances, and thus be able to process the transmitted data. However, there are only a few antennas of this type in the world, as they are technically complex and expensive to build.

For operations within the Artemis program, the two Deep Space Networks of NASA and ESA, as well as the Deep Space Antenna of DLR, are intended to be used. The NASA antennas are located approximately 120 degrees apart in terms of longitude. The exact locations of the ground stations are Goldstone (USA), Madrid (Spain), and Canberra (Australia). This ensures that, despite Earth's rotation, a communication link to a specific point in space is always possible. The NASA network is called the *Deep Space Network* (DSN) [40]. Photos of the three mentioned ground stations can be seen in figure 4.1.

(a) (b) (c)

Figure 4.1: Photos of the Deep Space Network ground stations Canberra (a), Goldstone (b), and Madrid (c) of NASA [13]

However, in the event of a ground station failure, the antennas of ESA are used as redundancy. These antennas are called *Deep Space Antennas* (DSA) and are also located at 120-degree intervals in terms of longitude. ESA has chosen the locations Cebreros (Spain), Malargüe (Argentina), and New Norcia (Australia) for its ground stations. Photos of the three stations are shown in figure 4.2.

(a) (b) (c)

Figure 4.2: Photos of the Deep Space Antennas ground stations Cebreros (a) [14], Malargüe (b) [15], and New Norcia (c) [16] of ESA

In addition to these six antennas, the largest antenna of the DLR ground station in Weilheim is also intended to be used. This 30-meter diameter antenna is also capable of establishing a connection to distant objects. The entire ground station is shown in figure 4.3. Figure 4.4 displays the 30-meter antenna.

Figure 4.3: Photo of the DLR ground station in Weilheim [17]

Figure 4.4: Photo of the 30-meter antenna of the DLR ground station in Weilheim [17]

Since the large antennas are needed to receive signals from distant spacecraft, it should be mentioned that the issue of attenuation does not arise when data is transmitted from the control center to the spacecraft. The reason for this is that the ground stations have a very high electrical power. Accordingly, the signals are sufficiently strong to be easily received by the spacecraft, even with a small antenna.

4.2.2 Analysis of the transfers

After presenting the ground stations used in the Artemis program, let's now analyze the communication link between the spacecraft and the control center during the transfers using these ground stations. We will examine the transfers presented in chapters 3.4.1 to 3.4.3.

The analysis is performed using graphs that depict the elevation angle of the spacecraft above the local horizon of each ground station during the transfers. If the elevation angle is below 5 degrees, communication is hardly possible. If the elevation angle is 0 degrees or not specified for a specific ground station at a certain time during the transfer, it means that the spacecraft is at a point in space that is not visible from the location of the ground station on Earth's surface. Therefore, that ground station cannot be used at that time to establish a connection between the spacecraft and the control center. The graphs are automatically generated by the DLR internal Fortran tool called *ORI* based on the results of the calculations. Table 4.2 shows the abbreviations (IDs) of the ground stations used in the following diagrams.

ORI ID	CNB43	GDS14	MAD63	WHM1	PRTH	CEBR	MALA
Name	Canberra	Goldstone	Madrid	Weilheim	New Norcia	Cebreros	Malargüe

Table 4.2: Table explaining the ORI IDs of the ground stations in the following diagrams

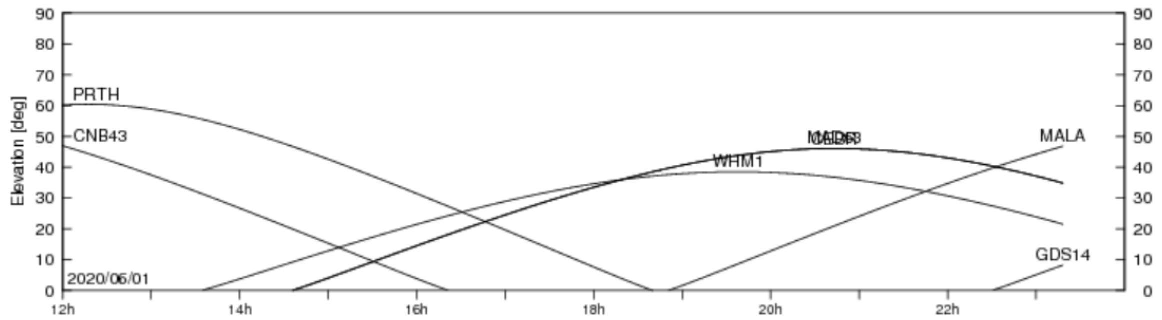

Figure 4.5: Diagram of the elevation angles of the spacecraft relative to each respective ground station during the transfer from NRHO (CR3BP) to LLO 1, starting at epoch 01.06.2020 12:00:00.000

Figure 4.5 depicts the aforementioned diagram for the transfer from the NRHO of the Gateway, calculated in the CR3BP, to the LLO 1 presented in chapter 3.2. It can be observed that at every point of the transfer, at least one ground station has an elevation angle greater than 30 degrees. Consequently, a connection between the control center and the spacecraft can be established at any time during this transfer.

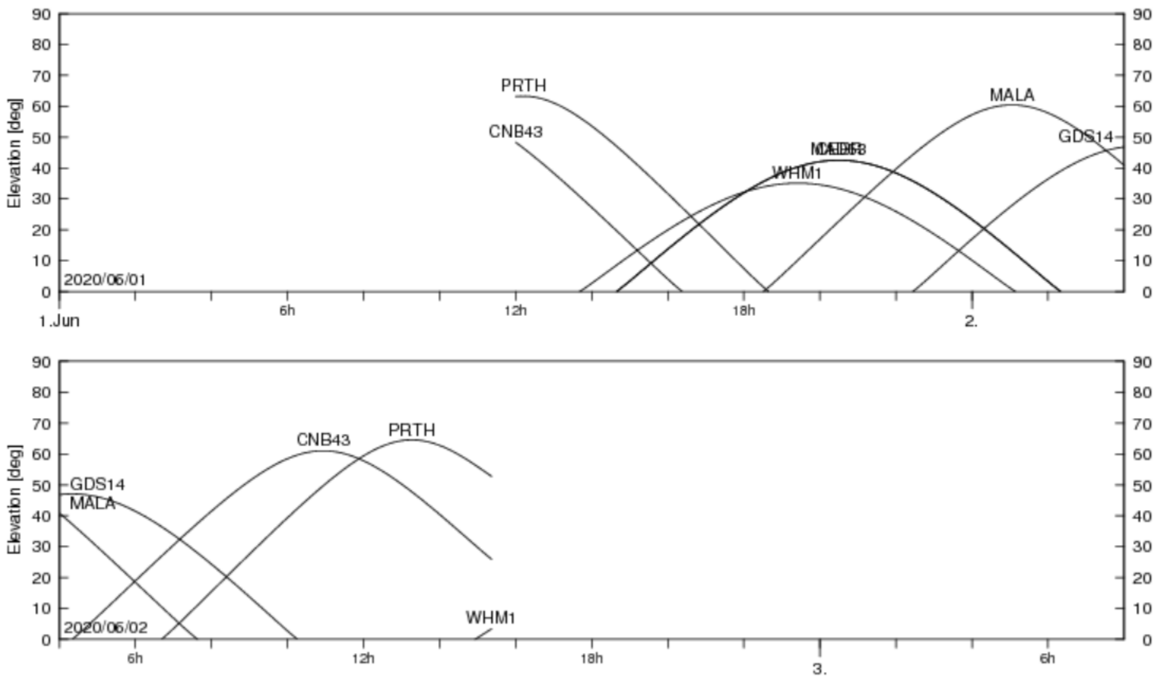

Figure 4.6: Diagram of the elevation angles of the spacecraft relative to each respective ground station during the transfer from NRHO (ephemerides) to LLO 1, starting at epoch 01.06.2020 12:00:00.000

Figure 4.6 presents the results for the transfer from the Gateway's orbit (ephemerides) to LLO 1. In this case, the diagram spans two rows as the transfer extends over two calendar days. Similarly to the previous case, it can be observed that the elevation angle never drops below 30 degrees, ensuring continuous communication between the control center and the spacecraft.

After the transfer to LLO 1, the transfers from the NRHO of the Gateway to LLO 2 are examined. The corresponding elevation angles over the ground stations are depicted in figures 4.7 and 4.8. Figure 4.7 displays the results for the transfer from the Gateway's orbit (CR3BP) to LLO 2, while the second figure represents the communication possibilities during the transfer from the NRHO (ephemerides) to LLO 2.
Both diagrams clearly indicate that for the transfer to LLO 2, there is always at least one ground station with an elevation angle towards the spacecraft greater than 30 degrees at any given time, irrespective of whether the Gateway's orbit was computed in the CR3BP or using ephemerides.

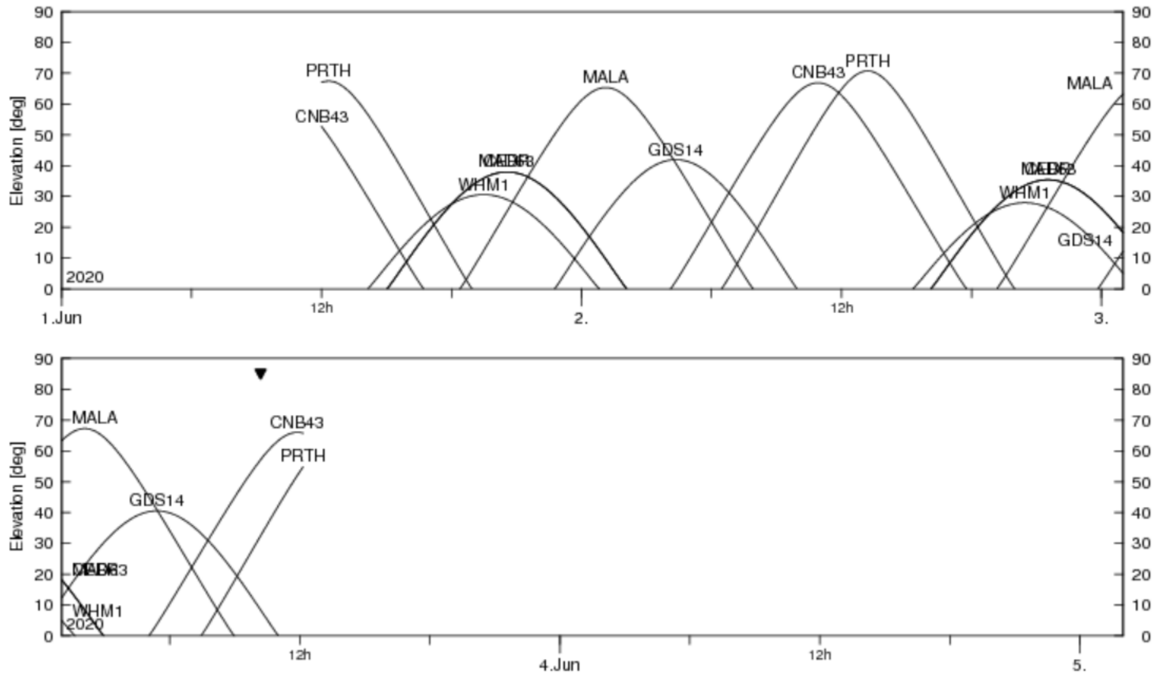

Figure 4.7: Diagram of the elevation angles of the spacecraft relative to each respective ground station during the transfer from NRHO (CR3BP) to LLO 2, starting at epoch 01.06.2020 12:00:00.000

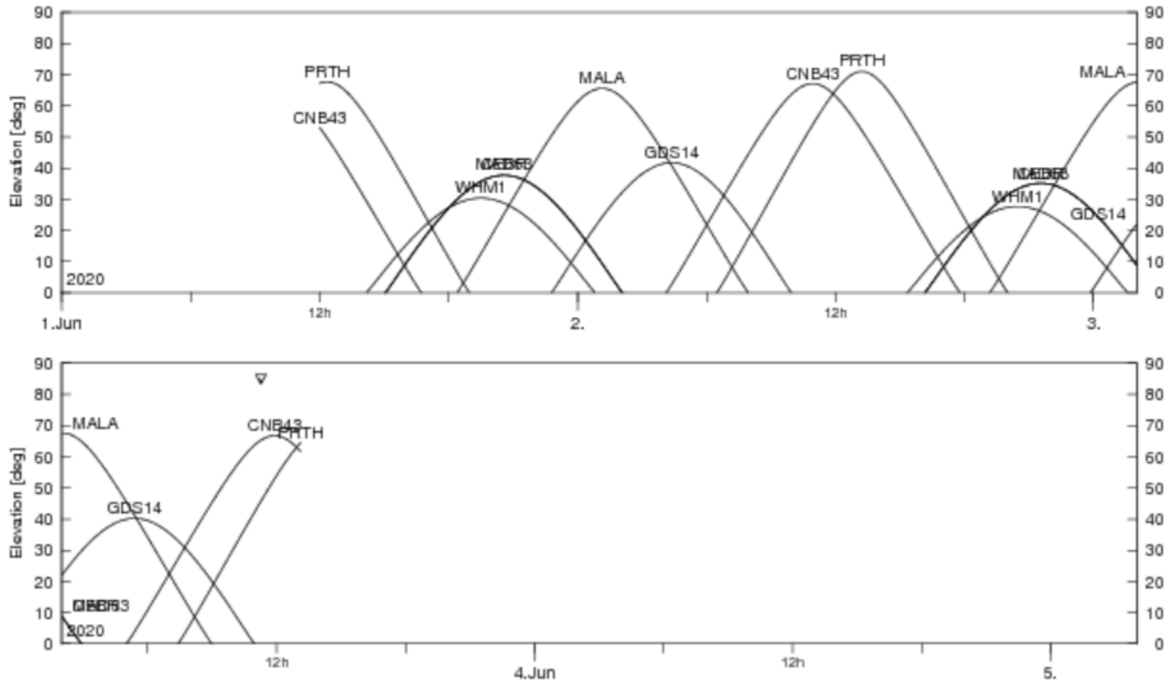

Figure 4.8: Diagram of the elevation angles of the spacecraft relative to each respective ground station during the transfer from NRHO (ephemerides) to LLO 2, starting at epoch 01.06.2020 12:00:00.000

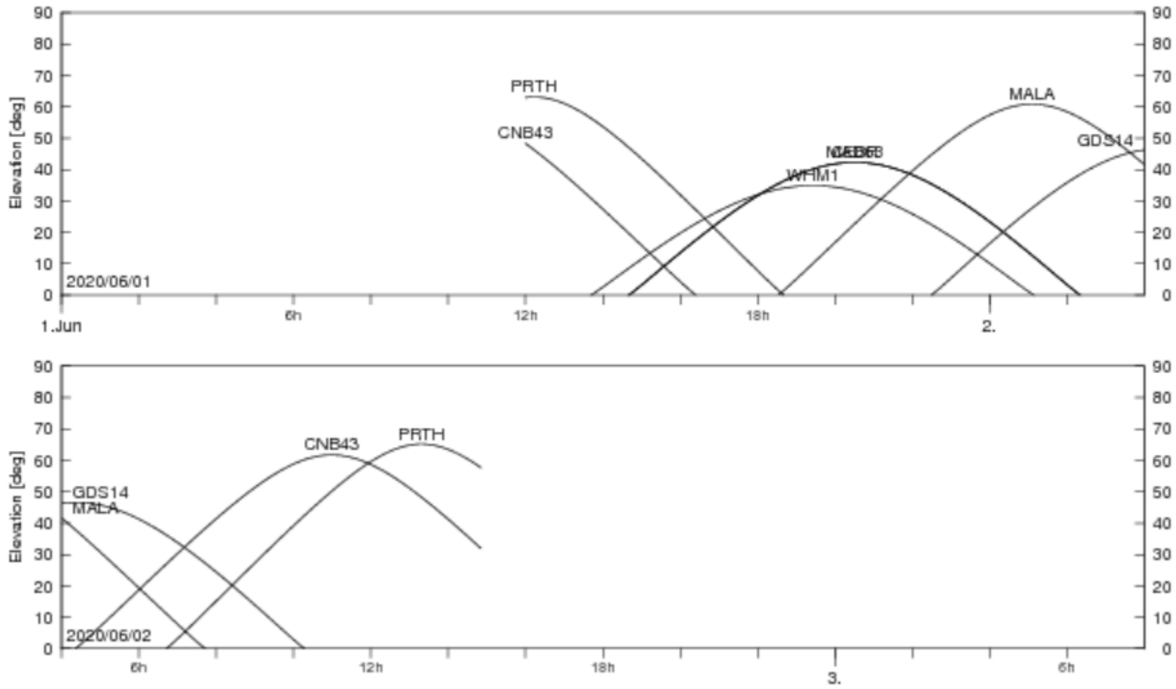

Figure 4.9: Diagram of the elevation angles of the spacecraft relative to each respective ground station during the transfer from NRHO (CR3BP) to LLO 3, starting at epoch 01.06.2020 12:00:00.000

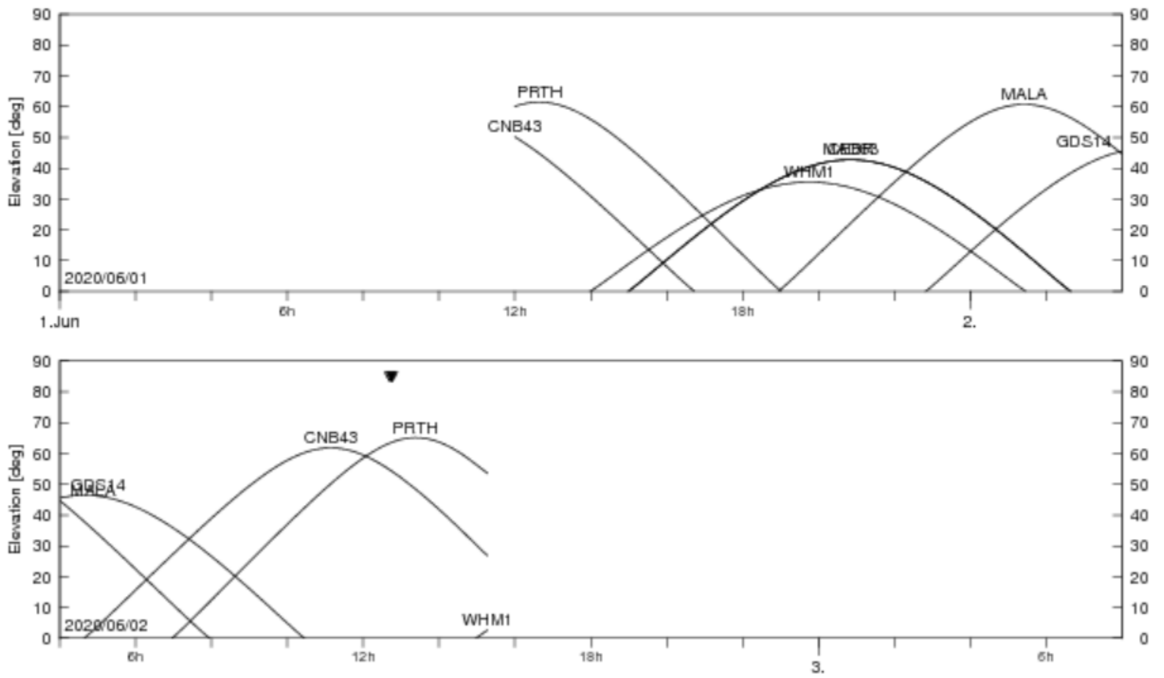

Figure 4.10: Diagram of the elevation angles of the spacecraft relative to each respective ground station during the transfer from NRHO (ephemerides) to LLO 3, starting at epoch 01.06.2020 12:00:00.000

Similarly, in figures 4.9 and 4.10, which depict the results for the transfer from the NRHO of the Gateway computed in the CR3BP and using ephemerides, respectively, to LLO 3, we observe similar outcomes. In both cases, the elevation angle towards at least one ground station remains above 30 degrees at all times. Consequently, continuous communication with the control center is possible during the transfer to LLO 3 as well.
Despite the continuous elevation angles of more than 5 degrees towards at least one ground station, it should be noted that communication outages can still occur during transfers and subsequently at the Lunar Lagrange orbits (LLOs). This is because communication is not possible when the Moon is positioned between the spacecraft and the ground station. Depending on the position of the LLOs, communication disruptions of up to half of the LLO's orbital period can therefore occur.

4.2.3 Evaluation of the results

Despite the positive results regarding the communication link during the transfers presented in the previous chapter (chapter 4.2.2), they should also be critically evaluated. For this purpose, we refer to the plots of the transfers presented in chapters 3.4.1 to 3.4.3 as a reference.
In figures 3.14 and 3.15, it is evident that the trajectories of the transfer to LLO 2 pass behind the Moon or even through the Lunar surface near the end of the transfer, from the perspective of Earth. This can be inferred from the location of the L2 point, whose position relative to the NRHO is shown in figure 3.3 (c). The same applies to the transfer to LLO 3, which is depicted in figure 3.17. Here as well, the trajectory passes behind the Moon before eventually passing through the Lunar surface.
For a communication link between the control center and the spacecraft using a ground station, a direct line of sight between the ground station antenna and the spacecraft is necessary. However, this is not the case when there is a celestial body in the line of sight. In the present case, this celestial body is the Moon. Therefore, when the transfer trajectory passes behind the Moon, a communication link cannot be established. As a result, for the cases of LLO 2 to NRHO (CR3BP and ephemerides) and LLO 3 to NRHO (ephemerides), there is no communication link at the end of the transfer.
The reason why this issue does not appear in the results from ORI is likely because the position of the Moon and the associated shadow region are not taken into account in ORI.

4.3 Eclipses

The third part of the operational analysis of the transfer trajectories focuses on the calculation of possible eclipses by the Moon or the Earth during the transfers. For this analysis, the Fortran tool ORI is used, similar to the analysis of the communication link (see chapter 4.2). In conjunction with ORI, the OEM files of the transfer trajectories generated by the code during the calculations (see chapters 3.3 and 3.4) are used to determine whether eclipses occur during each transfer.

The results of the calculations are presented by ORI in a bar chart. The bar chart for the transfer from NRHO (CR3BP) to LLO 1 is shown in figure 4.11. Only the two rows *EARTH* and *MOON* are relevant, as they represent the eclipses caused by the Earth and the Moon, respectively. As explained in chapter 3.1, eclipses are primarily a challenge for the power supply and thermal systems from an operational perspective. Therefore, it is best if no eclipses occur during a transfer, as this reduces the stress on the spacecraft and makes the transfer safer. This is especially relevant for manned transfers. Figure 4.11 shows that no eclipses occur during the entire transfer.

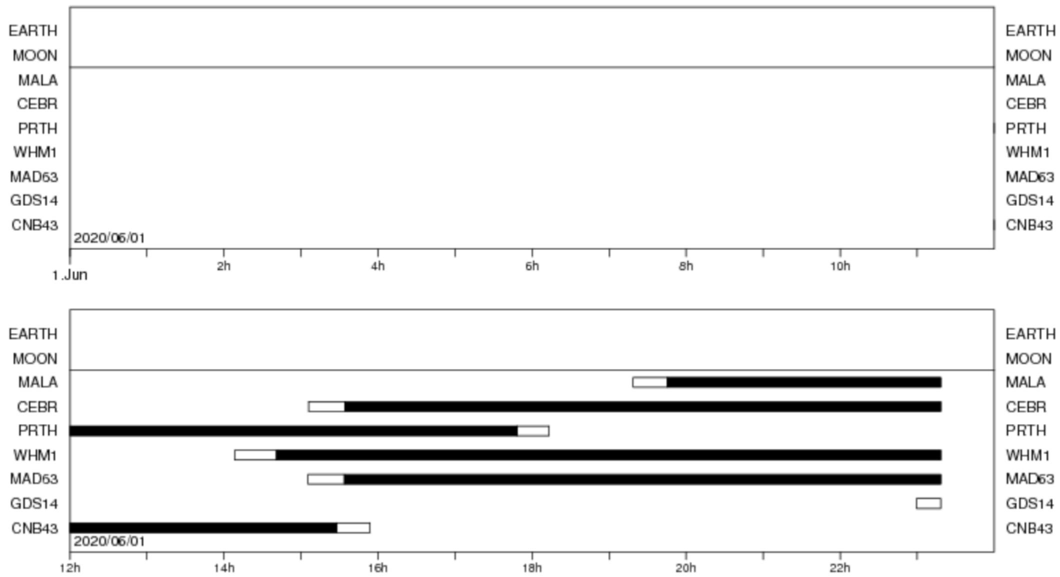

Figure 4.11: Bar chart of eclipses by Earth and Moon during the transfer from NRHO (CR3BP) to LLO 1 with the start epoch of 01.06.2020 12:00:00.000

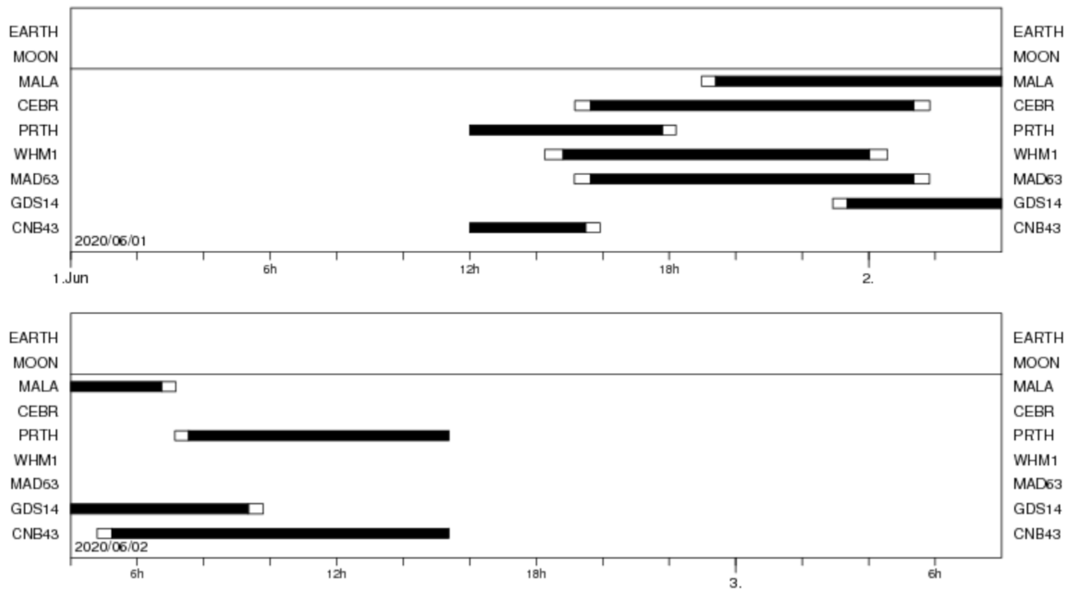

Figure 4.12: Bar chart of eclipses by Earth and Moon during the transfer from NRHO (ephemerides) to LLO 1 with the start epoch of 01.06.2020 12:00:00.000

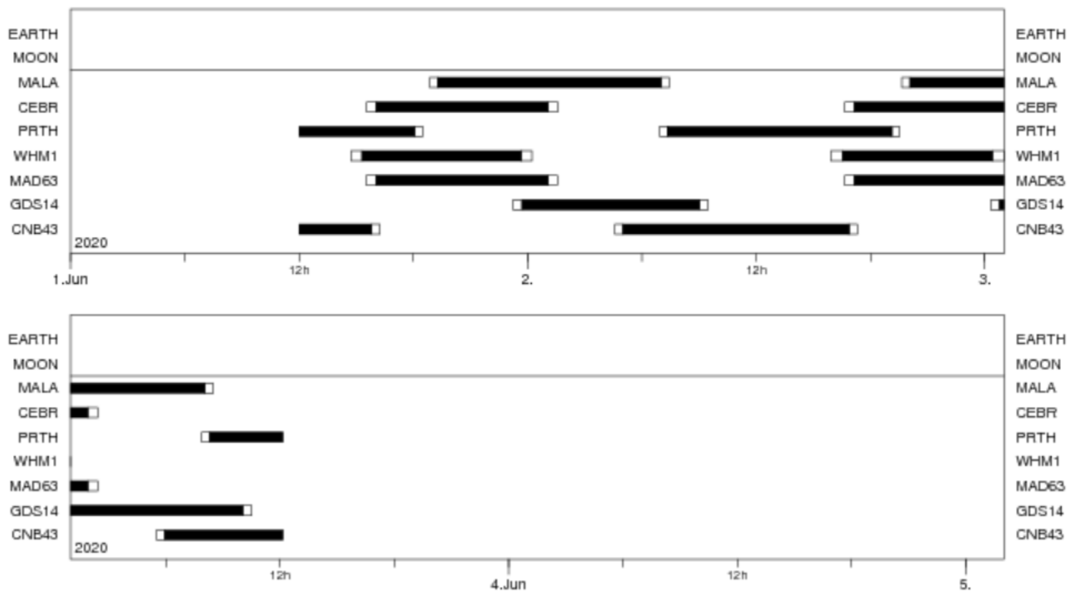

Figure 4.13: Bar chart of eclipses by Earth and Moon during the transfer from NRHO (CR3BP) to LLO 2 with the start epoch of 01.06.2020 12:00:00.000

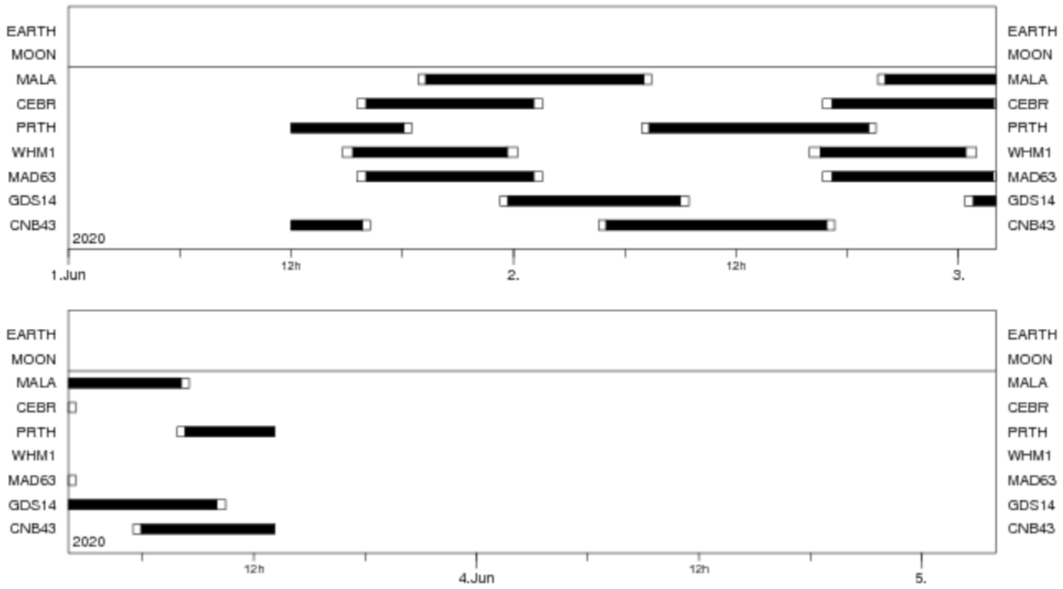

Figure 4.14: Bar chart of eclipses by Earth and Moon during the transfer from NRHO (ephemerides) to LLO 2 with the start epoch of 01.06.2020 12:00:00.000

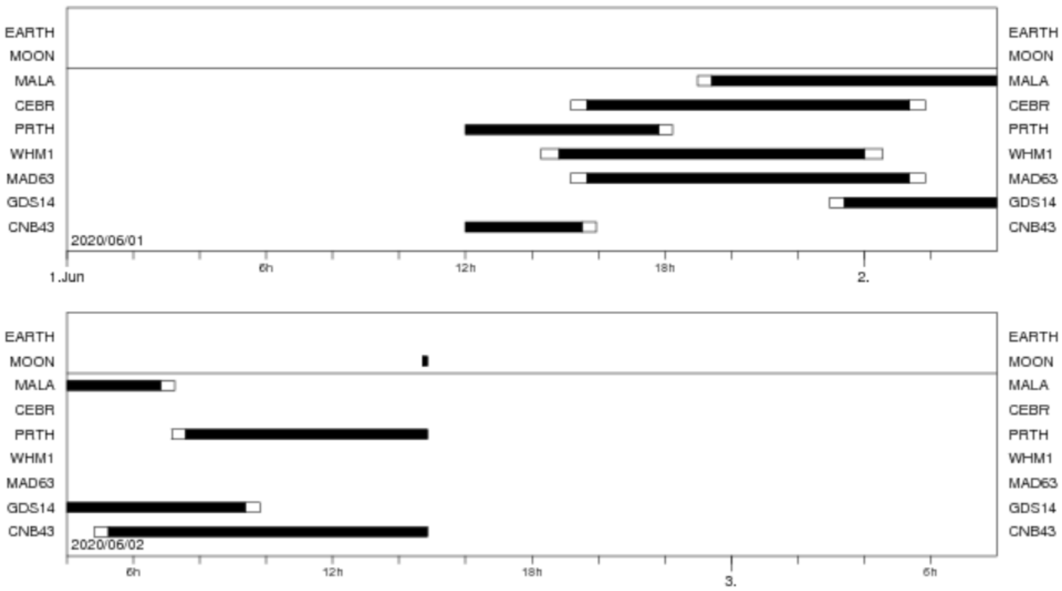

Figure 4.15: Bar chart of eclipses by Earth and Moon during the transfer from NRHO (CR3BP) to LLO 3 with the start epoch of 01.06.2020 12:00:00.000

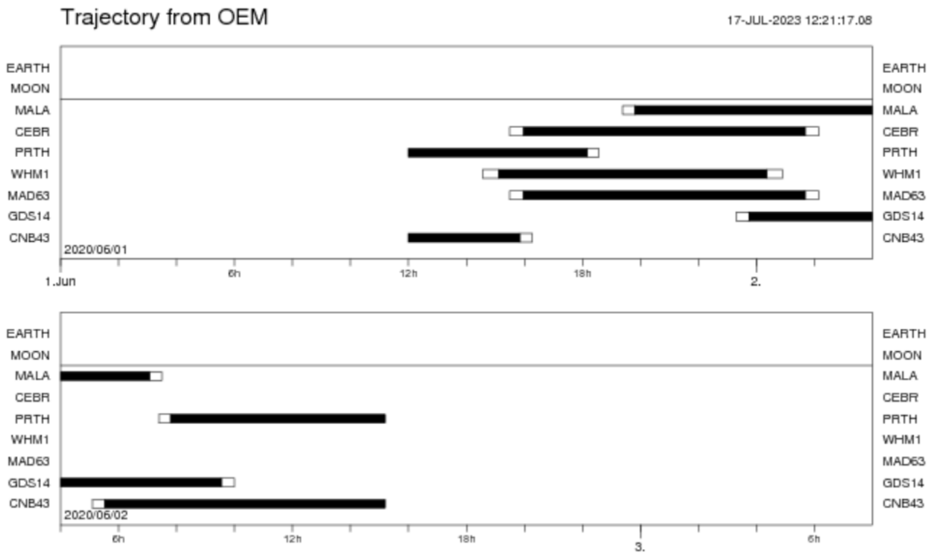

Figure 4.16: Bar chart of eclipses by Earth and Moon during the transfer from NRHO (ephemerides) to LLO 3 with the start epoch of 01.06.2020 12:00:00.000

The remaining transfer trajectories analyzed in chapters 3.4.1 to 3.4.3 are NRHO (ephemerides) to LLO 1, NRHO (CR3BP) to LLO 2, NRHO (ephemerides) to LLO 2, NRHO (CR3BP) to LLO 3, and NRHO (ephemerides) to LLO 3. The results of these cases are shown in figures 4.12 to 4.16 in the same order as listed. In all figures, except for one minor exception, it can be seen that no eclipses by the Earth or the Moon occur during the entire transfers.
The exception occurs at the end of the transfer from NRHO (CR3BP) to LLO 3, where a brief eclipse by the Moon takes place. Since this interval lasts only a few minutes, it does not pose a significant impact on the transfer itself. Nevertheless, in the case of performing this transfer, it should be verified whether the eclipse continues on LLO 3 and subsequently causes any disruptions.
In conclusion, it can be stated that eclipses by the Earth and the Moon do not pose any significant impact on the calculated transfers and the selected epoch. However, these results are strongly dependent on the start epoch and should be re-evaluated for the exact start epoch in a real mission to exclude any potential disruptions.

All in all, it can be summarized that the calculated transfer trajectories are feasible for manned spacecraft from an operational perspective. The communication windows are sufficiently large, the flight durations do not exceed the set limit of 3 days, and there are minimal occurrences of eclipses.

Chapter 5

Résumé

5.1 Conclusion

After conducting the analyses and calculations as described earlier, the findings and results are summarized.

Within this work, descent trajectories from the Gateway's NRHO to the Lunar surface were analyzed from both orbital mechanics and operational perspectives. This was achieved by dividing the descent into two stages. The first stage consists of transfer trajectories from the Gateway's orbit to a LLO. For the analyses, three circular Kepler orbits at an altitude of 100 km above the Lunar surface were selected. The orbital planes of these three orbits were chosen to be orthogonal to each other to examine a wide range of orbits. Calculations and optimizations of the descent trajectories were performed using the open-source software SEMpy. This required adjusting the existing scripts and adding additional functionalities. The calculations of the transfer trajectories from the Gateway NRHO to the three selected LLOs were perfomed both in the CR3BP model and in the high-fidelity ephemeris model. To cross-check the sanity of the computed trajectories, the latter were visualised using the independent FreeFlyer Tool of a.i. solutions.

In the second stage, the descent from the LLOs to the Lunar surface was described based on theoretical considerations and literature sources. The steps of the descent are independent of the choice of LLO, including the required change in velocity for this part of the descent.

After completing the calculations, two case studies were conducted to contextualize the results. The feasibility of the calculated transfers was assessed using both the NASA Orion capsule and the SpaceX Starship. It was demonstrated that the transfers to two out of the three LLOs are feasible with both spacecraft, provided refueling at the Gateway before the transfer is possible. The Starship is even capable of performing a transfer to an LLO coplanar with the NRHO and handling the descent and ascent from and to the Lunar surface. This also requires refueling after the transfer from Earth to the Gateway with a sufficient amount of propellant. Some of these calculations were based on official values, while others were based on publicly available non-official values.

In addition to the orbital mechanics analyses and the assessment of propellant requirements, operational aspects of the calculated trajectories were also investigated. For this purpose, the calculated transfer trajectories had to be represented in the OEM format. This was necessary to utilize the Fortran tool ORI developed by DLR. The tool is capable of calculating communication windows with specific ground stations and determining eclipses caused by the Earth or the Moon using a given trajectory in the OEM format.
The results showed that continuous communication with the control center is possible during the transfers due to the utilization of deep space antennas from ESA, NASA, and DLR. However, it should be noted that communication is not possible when the spacecraft is behind the Moon from Earth's perspective. The investigation of eclipses also yielded positive results for all three trajectories. Nevertheless, it is important to consider that, depending on the location of the LLO after arrival, there may be an eclipse duration of nearly half an orbit period.
In addition to communication and eclipse analysis, the flight duration of each transfer was also examined. As the longest flight takes a little over two days, this was deemed non-critical in the overall assessment.

In conclusion, based on the results of this work, it can be inferred that the descent from the Gateway to the Moon is feasible using the Starship or a combination of the Orion capsule and a lander module. To minimize propellant consumption, a polar LLO should be chosen. If a plane change is required during the transfer from the NRHO to the respective LLO, it is advisable to execute it as close to the NRHO's apocenter as possible, as the spacecraft's velocity and, consequently, the propellant requirements for the maneuver are lowest there.

5.2 Outlook

As described in chapter 5.1, all objectives of the work have been achieved. Nevertheless, for a more detailed mission analysis, some points should be further investigated.

One of these points is the use of point mass models for Earth and the Moon. It is essential to examine whether and to what extent a more accurate gravity field and mass model could influence the results.
In addition, other optimization algorithms could be explored to potentially find even better transfer trajectories. One suggestion would be to use a global optimizer. In this work, only the local optimizer *Cobyla* was used. The abbreviation *Cobyla* stands for **C**onstrained **O**ptimization **BY L**inear **A**pproximation [41]. This means that when considering alternative solutions, the algorithm chooses the closest local minimum. On the other hand, a global optimizer would find the absolute (global) minimum in the complete search space.
Another point necessary for the implementation of the transfers in the context of a real mission is the precise planning of maneuvers. As the calculated impulses are sometimes more than 1000 $\frac{m}{s}$, they cannot be generated in a short time interval in reality. Therefore, it would be necessary to investigate which sequence of maneuvers would be required to fly the calculated trajectories with the spacecraft's propulsion systems and how the required ignition times would affect the shape of the transfer orbits. In connection with this, it is also important to analyze the consequences of small ignition errors. For very large maneuvers, even small percentage errors have a significant influence on the flown trajectory.

By considering these points and other mission-specific aspects in conjunction with the results of this work, a descent from the Gateway's orbit to the Lunar surface on the calculated trajectories would indeed be feasible.

Appendix

Bibliography

[1] F. Sellmaier, T. Uhlig, and M. Schmidhuber, *Spacecraft Operations*, 2nd ed., ser. Springer Aerospace Technology. Springer International Publishing and Springer, 2022.

[2] D. de la Torre Sangrà and E. Fantino, *Review of Lambert's Problem*. arXiv, 2021.

[3] P. Davis, S. Carney, B. Dunford, and M. Boeck. (2023) Earth's Moon. Planetary Science Communications team - NASA's Jet Propulsion Laboratory. [Online]. Available: https://solarsystem.nasa.gov/moons/earths-moon/overview/

[4] ESA. (2022) Earth. EUMETSAT/ESA. [Online]. Available: https://www.esa.int/Space_in_Member_States/Germany/WeltraumWagner-Podcast_live_mit_ESA_EUMETSAT_Weltraummissionen_die_den_Puls_unseres_Planeten_fuehlen

[5] E. Blazquez, P. Guardabasso, T. Gateau, and A. Fossa, "SEMpy," Institut Supérieur de l'Aéronautique et de l'Espace, 2021. [Online]. Available: https://gitlab.isae-supaero.fr/sempy

[6] E. M. Zimovan, K. C. Howell, and D. C. Davis, *Near Rectilinear Halo Orbits and their application in cis-lunar space*, 2017. [Online]. Available: https://www.researchgate.net/publication/319531960

[7] D. E. Lee, *White Paper: Gateway Destination Orbit Model:*, 2019.

[8] J. S. Parker and R. L. Anderson, *Low-Energy Lunar Tajectory Design*, 2013. [Online]. Available: https://descanso.jpl.nasa.gov/monograph/series12/LunarTraj--Overall.pdf

[9] R. R. Sostaric and J. R. Rea, *Powered Descent Guidance Methods for the Moon and Mars*, 2005. [Online]. Available: https://arc.aiaa.org/doi/pdf/10.2514/6.2005-6287

[10] NASA Johnson Space Center, *ORION*.

[11] Flickr. (01.05.2023) Starship Test Flight Mission. [Online]. Available: https://www.flickr.com/photos/spacex/52822653368/

[12] SpaceX. (27.04.2023) SpaceX. [Online]. Available: https://www.spacex.com/vehicles/starship/

[13] T. Mai. (2017) Deep Space Network's 50th Anniversary. NASA. [Online]. Available: https://www.nasa.gov/directorates/heo/scan/news_DSN_50th_Anniversary.html

[14] ESA. (2005) General view of Cebreros. ESA. [Online]. Available: https://www.esa.int/Enabling_Support/Operations/ESA_Ground_Stations/Cebreros_inaugurated_ready_for_Venus_Express

[15] D. Pazos. (2016) Comet relay. ESA. [Online]. Available: https://www.esa.int/Enabling_Support/Operations/ESA_Ground_Stations/Malarguee_-_DSA_3

[16] D. O'Donnell. (2018) ESA's solar-powered giant one year on. ESA. [Online]. Available: https://www.esa.int/Enabling_Support/Operations/ESA_Ground_Stations/Highlights/Tracking_station_gallery

[17] B. Jung. Weilheim. DLR. [Online]. Available: https://www.dlr.de/en/dlr/locations-and-offices/weilheim

[18] J. A. Kegerreis, S. Ruiz-Bonilla, V. R. Eke, R. J. Massey, T. D. Sandnes, and L. F. A. Teodoro, *Immediate Origin of the Moon as a Post-impact Satellite*. American Astronomical Society, 2022.

[19] J. Uri. (2019) 50 Years Ago: One Small Step, One Giant Leap. [Online]. Available: https://www.nasa.gov/feature/50-years-ago-one-small-step-one-giant-leap

[20] B. Dunbar. (2021) What is Artemis? NASA. [Online]. Available: https://www.nasa.gov/what-is-artemis

[21] S. Creech, J. Guidi, and D. Elburn, *Artemis*. IEEE, 2022.

[22] A. Malcherek, *Elektromagnetismus und Gravitation*, 1st ed. Springer Fachmedien Wiesbaden and Springer Vieweg, 2022, malcherek, Andreas (Verfasser.).

[23] Oxford Reference. first point of Aries. [Online]. Available: https://www.oxfordreference.com/display/10.1093/oi/authority.20110803095820164;jsessionid=F9D2C4C139ED2A97D36EEABCCD300905

[24] R. W. Easton, R. L. Anderson, and M. W. Lo, *An Elementary Solution To Lambert's Problem*. arXiv, 2021.

[25] R. P. Russell, *On the solution to every Lambert Problem*. Springer, 2019.

[26] J.-L. Lagrange, *Mécanique Analytique*, ser. Cambridge Library Collection - Mathematics. Cambridge University Press, 2009.

[27] C. H. Davis, *Theory of the Motion of the heavenly bodies moving about the sun in conic sections*, 1965.

[28] D. Zuehlke, Y. Taylor, D. Posada, J. Nicolich, C. W. Hays, A. Malik, and T. Henderson, *Initial orbit determination for the CR3BP using particle swarm optimization.* arXiv, 2022.

[29] E. M. Zimovan-Spreen, K. C. Howell, and D. C. Davis, *Dynamical structures nearby NRHOs with applications to transfer design in cislunar space.* Springer, 2022.

[30] R. Park. Description of Orbits and Ephemerides. Jet Propulsion Laboratory, California Institute of Technology, NASA. [Online]. Available: https://ssd.jpl.nasa.gov/orbits_doc.html

[31] W. S. Koon, M. W. Lo, J. E. Marsden, and S. D. Ross, *Dynamical Systems, the Three-Body Problem and Space Mission Design*, 2011. [Online]. Available: http://www.cds.caltech.edu/~marsden/books/Mission_Design.html

[32] J. Williams, D. E. Lee, R. J. Whitley, K. A. Bokelmann, D. C. Davis, and C. F. Berry, *Targeting cislunar Near Rectilinear Halo Orbits for Human Space Exploration*, 2017. [Online]. Available: https://ntrs.nasa.gov/citations/20170001352

[33] R. Whitley and R. Martinez, *Options for Staging Orbits in Cislunar Space*, 2010. [Online]. Available: https://ieeexplore.ieee.org/abstract/document/7500635

[34] R. J. Whitley, D. C. Davis, L. M. Burke, B. P. McCarthy, R. J. Power, M. L. McGuire, and K. C. Howell, *Earth-Moon Near Rectilinear Halo and Butterfly Orbits for lunar surface exploration*, 2018. [Online]. Available: https://www.researchgate.net/profile/Brian-Mccarthy-11/publication/339028625_Earth-Moon_Near_Rectilinear_Halo_and_Butterfly_Orbits_for_Lunar_Surface_Exploration/links/5fb68a7e299bf104cf5b9199/Earth-Moon-Near-Rectilinear-Halo-and-Butterfly-Orbits-for-Lunar-Surface-Exploration.pdf

[35] J. Condon, *First Lunar Outpost Powered Descent Design and Performance*, 1992.

[36] (28.04.2023) Propulsion. [Online]. Available: https://www.esa.int/Science_Exploration/Human_and_Robotic_Exploration/Orion/Propulsion

[37] Wikipedia. (2023) Orbital Maneuvering System. [Online]. Available: https://en.wikipedia.org/wiki/Orbital_Maneuvering_System

[38] ——. (2023) SpaceX Raptor. [Online]. Available: https://en.wikipedia.org/wiki/SpaceX_Raptor

[39] ——. (2023) SpaceX Starship. [Online]. Available: https://en.wikipedia.org/wiki/SpaceX_Starship

[40] H. Monaghan. (2022) What is the Deep Space Network? Jet Propulsion Laboratory, NASA. [Online]. Available: https://www.nasa.gov/directorates/heo/scan/services/networks/deep_space_network/about

[41] D. Izzo and F. Biscani. (2015) PyGMO. ESA. [Online]. Available: https://esa.github.io/pygmo/documentation/algorithms.html#PyGMO.algorithm.nlopt_cobyla